STUDY OF THE EFFECT OF BRAZING ON MECHANICAL PROPERTIES OF ALUMINUM ALLOYS FOR AUTOMOTIVE HEAT EXCHANGERS

A Thesis

Submitted to the Faculty

of

Purdue University

by

Praveen Kumaar Velu

In Partial Fulfillment of the

Requirements for the Degree

of

Master of Science in Mechanical Engineering

May 2017

Purdue University

Indianapolis, Indiana

THE PURDUE UNIVERSITY GRADUATE SCHOOL
STATEMENT OF THESIS APPROVAL

Dr. Hazim El-Mounayri, Chair

Associate Professor of Mechanical Engineering

Dr. Andres Tovar

Assistant Professor of Mechanical Engineering

Dr. Jing Zhang

Assistant Professor of Mechanical Engineering

Approved by:

Dr. Sohel Anwar

Head of the Departmental Graduate Program

To my Parents.

ACKNOWLEDGMENTS

I would like to thank my parents for their unconditional love and unrelenting support for my endeavors.

I would like to express my sincere gratitude to my advisor, Dr.Hazim El-Mounayri for his guidance and professional support. I would also like to thank my supervisor at Valeo, James Hornsby for his continuous support, patience and motivation.

Most importantly I would like to thank Carl Hildinger, Anne-Gaelle Noumet-Villemiane, Nicolas Dye-Pellisson and Patrick Cameron for their most valuable training, guidance and knowledge shared to help me carry out my research successfully.

TABLE OF CONTENTS

Page

LIST OF TABLES

LIST OF FIGURES

ABSTRACT

Velu, Praveen Kumaar MSME, Purdue University, May 2017. Study of the Effect of Brazing on Mechanical Properties of Aluminum Alloys for Automotive Heat Exchangers. Major Professor: Dr. Hazim El-Mounayri.

Automotive heat exchangers enable the engine to operate at acceptable temperatures. The quality of these heat exchangers plays a key role in vehicle performance because they ensure the integrity of the engine, and can cause significant mechanical complications in case of malfunction.

From manufacturing stand point view, the general behavior of the structure in controlling the various modes of damage to heat exchangers becomes an indisputable challenge (influence of the process assembly, design, etc.). The evolution of materials used, in particular through the different alloy types, brazing operational parameters and part designs could be used to tackle these challenges. This imposes the constant need to control the conditions of use and to understand the braze alloy mechanisms to provide the best possible solutions for manufacturing automotive heat exchangers. An experimental study is conducted by simulating the brazing of alloys and the mechanical properties after brazing as well as re-brazing. Aluminum alloys with different compositions and metallurgical conditions that are used in the automotive heat exchanger industry are used in this study to understand the effect of brazing on the mechanical properties. The experiments conducted and results obtained show the degradation in the mechanical properties after brazing. But interestingly the mechanical properties of the re-brazed alloys studied are very similar to the first brazing cycle. This generates further interest in exploring more about the mechanical properties of re-brazed alloy and their feasibility in industrial process.

1. INTRODUCTION

1.1 Background

From the introduction of the history of cars to the mid-1970's, radiators produced using copper and brass were in all of the automotive industry. The second generation of radiators were shifting towards water cooled engine from air cooled engines. Later critical calls for approaches to decrease fuel utilization, automotive manufacturers started making autos and trucks with lighter materials. For radiators made by aluminum, with thickness lesser than copper/brass can deal with heat better in spite of its numerous inadequacies. In its crude state (in spite of the fact that not as radiator strip), aluminum is additionally less costly. These qualities alongside a critical, though hidden forecasts of product examiners was that copper/brass would be hard to come by in the 1980s - made an influx of energy for something new. In the recent years, the Automotive heat exchangers for Engine cooling systems and also for the heating, ventilation and air-conditioning systems are made by Aluminum. Due to some interesting properties like high thermal conductivity, low density, relatively good corrosion resistance possessed by Aluminum alloys helps them achieve high part product performance, production efficiencies and are most predominantly used to make heat exchangers in the automotive industry [1]. Cooling radiators being the main focus of study in this research can be manufactured possibly in two different ways, by mechanical assembly or by brazing. Towards the end of 20th century, the mechanical assembly of automotive radiators was replaced by Aluminum brazing. This was a result of making progress toward a cost effective, safe and cleaner technology.

Driven by the tightening of anti-pollution standards and by economic constraints, the current trend of the automobile market is downsizing and the lightening of vehicles [2]. For the heat exchangers, this mass reduction is tried achieving through

the reduction of the thickness of the components [3]. This reduction in thickness, combined with the increase in mechanical stresses can lead to fatigue failure of the components and particularly of the tubes [4]. Even if corrosion phenomena are still a key factor to guarantee a long service life of materials, the limiting factor for the heat exchanger durability is now moving towards fatigue resistance of exchangers [5–7].

For about thirty years, Aluminum has become a constituent metal for exchangers and has in fact replaced metals such as cast iron and copper which were used for their excellent thermal properties [8,9]. The development of Aluminum is largely due to its lower density and specific mechanical properties (relative to the density) and therefore to the weight gain of the structures which it induces the heat exchangers contribute to meet the many environmental standards, in particular those requiring car manufacturers to reduce their CO_2 emissions. Easy implementation form of the Aluminum alloys, good resistance to corrosion and their fairly stable price (because of their relative abundance availability) enables them a wide use in industries.

Based on assembly method used the manufacture of heat exchangers can be of two types, mechanical assembly of components and in the other where the assembly is done by brazing. This study focuses exclusively on the second type of exchangers.

1.2 Heat Exchangers in Automotive Industry

In a vehicle, due to combustion of the fuel or various frictions between parts, the rise in temperature of the engine block is inevitable. The latter can quickly become a source of serious damage if it is not properly regulated. Conversely, too low temperature affects engine performance and causes premature wear. Such use also leads to a drastic fall in the duration life of parts. The need for good temperature regulation is therefore essential and requires the use of various heat exchangers, the number of which varies from 2 to 5 depending on the vehicle.

However irrespective of what type of exchanger is considered, the general structure remains the same. Only the design, component geometry and composition of the

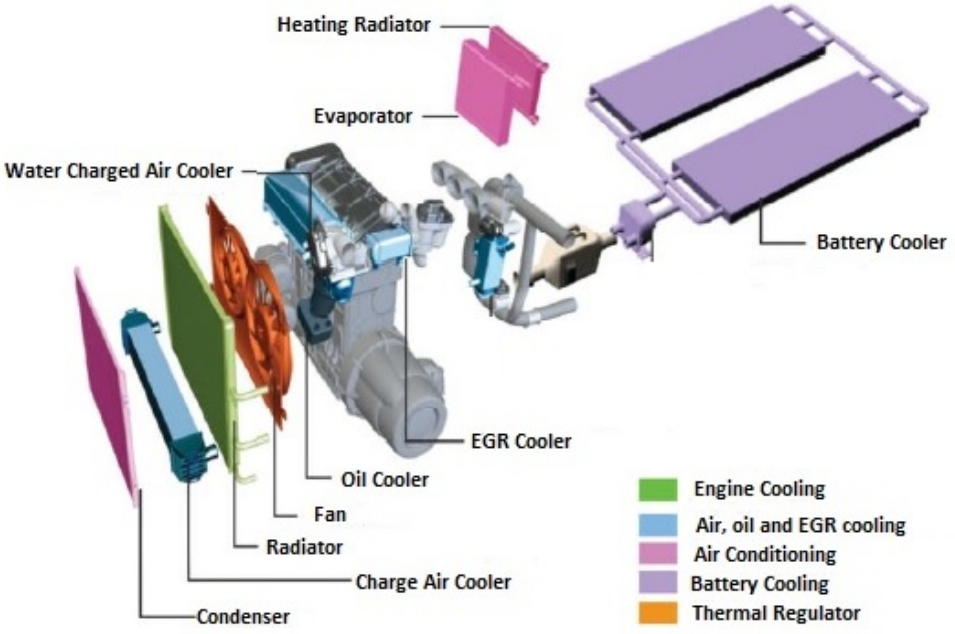

Fig. 1.1. Exploded diagrammatic view of the various heat exchangers that can be found on a motor vehicle.

constituent Aluminum alloys evolve according to the desired thermal capacities, the nature of the heat exchanges and the location of the exchanger in the engine part. Thus there are different types depending on the utility and the desired thermal control capacities. For the vast majority of vehicles, the various exchangers present in the engines are the following:

- Cooling Radiator
- Heating Radiator
- Charge Air Cooler
- Condenser
- Evaporator

The exchangers are grouped according to the cooling loop to which they belong are concerned. The engine circuit comprises a cooling radiator responsible for maintaining the temperature at an optimum level and a heating radiator which uses the heat produced by the engine to warm up the passenger compartment. To these two exchangers, an oil cooler is added in order to avoid a rise in temperature of the oil which would cause its degradation.

In the case of supercharged cars, the cooling of the intake gases is ensured by the charge air cooler. The supercharging device consists of a turbocharger (or mechanical compressor) directly driven by the engine that compresses the intake air. As a result of this compression, the intake air temperature is increased. However, a hot air is less dense which reduces the efficiency of the engine. The purpose of the charge air cooler is therefore to reduce the temperature of the compressed air.

EGR devices are used to reduce emissions of nitrogen oxides. The principle is to re-admit a portion of the exhaust gas to slow down the rate of combustion (one of the reasons being, addition of exhaust gas decreases the proportion of oxygen in the mixture and reduces the temperature during combustion). Before being re-admitted the exhaust gases must be cooled and it is accomplished by an EGR cooler. Depending on its position in the engine, it may operate at low or high pressure (EGR LP or HP).

The air conditioning system consists of two heat exchangers (condenser and evaporator). The condenser placed in front of the vehicle is responsible for evacuating the heat from the passenger compartment to the outside. The evaporator placed under the dashboard, diffuses a fresh and dry air in the cockpit. This loop uses the changes in the states of a heat transfer fluid and a compressor in order to perform heat exchanges.

1.2.1 Cooling Circuit

In the first stage of operation, the cooling circuit transfers the excess heat from the engine to the heat transfer fluid. Later the heat transfer fluid is cooled by air / liquid exchanges with the environment outside. This principle of operation remains the same regardless of the type of exchanger used.

The heat transfer fluid, also called the cooling liquid is maintained under pressure in a closed circuit. The water pump, driven by the engine timing belt, accelerates the circulation of this liquid with a focus to optimize the heat exchanges within the various components of the cooling circuit.

The thermostatic valve which is located close to the Engine, allows a regulation of the flow of liquid into the system. The cooling radiator is in charge of the dissipation of 75% of the energy balance. As shown in Fig. 1.2., the cooling radiator is associated with a motor-fan unit able to circulate air faster by convection, in order to promote heat exchanges.

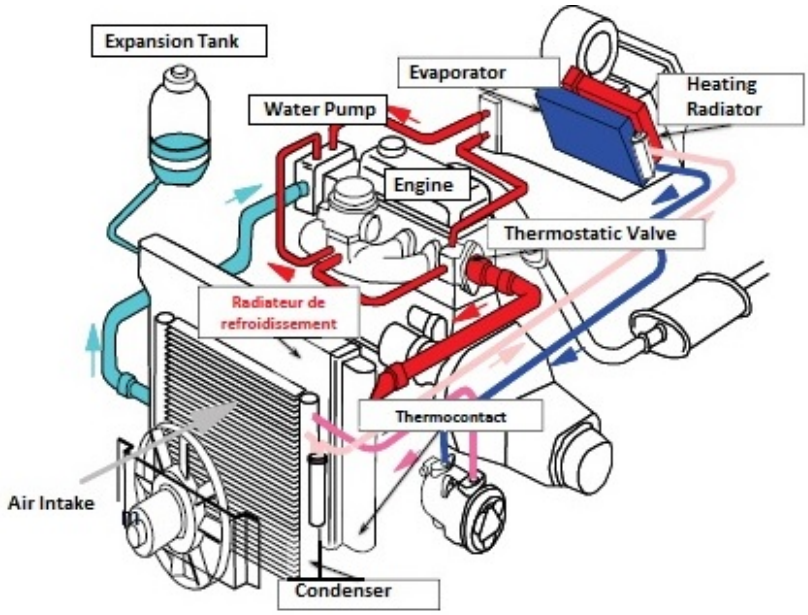

Fig. 1.2. Schematic view of an engine cooling system (without charge air cooler) associated with the air conditioning loop.

An exploded general view of a cooling radiator assembled by brazing technique is shown below (Fig. 3.1). This figure highlights the elements in the system and also the heat exchanges between the heat transfer fluid and the external medium. The brazing ensures the good performance of the assembly. The tank being only a polymer element for certain heat exchangers makes it possible to ensure the leak tightness of the device with the crimping of the header to it.

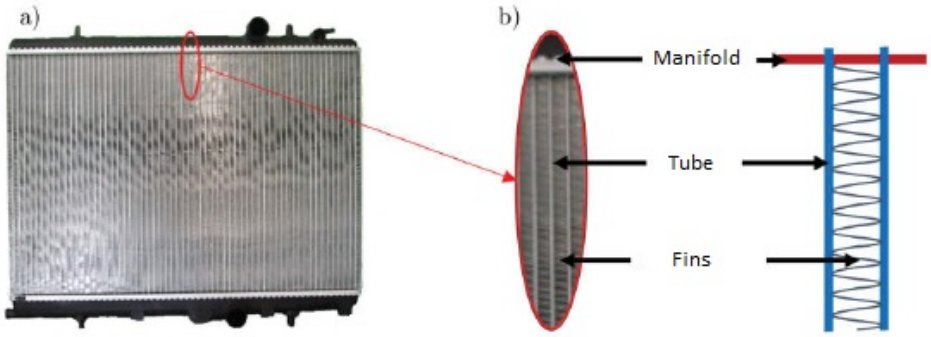

Fig. 1.3. Structure of a cooling radiator - a) Radiator, b) Enlarged schematic representation

1.2.2 Heat Exchange Mechanisms

Thermal exchanges take place in the vast majority within the radiator. These exchanges can be divided into three distinct stages (Fig. 1.4.):

1. The heat transfer fluid transmits excess heat from the engine by convection to the inner wall of the tube.

2. The heat transmitted to the tube is propagated by conduction through the thickness of the tubes up to the dividers. This spread is facilitated by the strong contact between components induced by the brazing process.

3. The external wall of the tube and the interlayer provide the heat transfer to ambient air by convection.

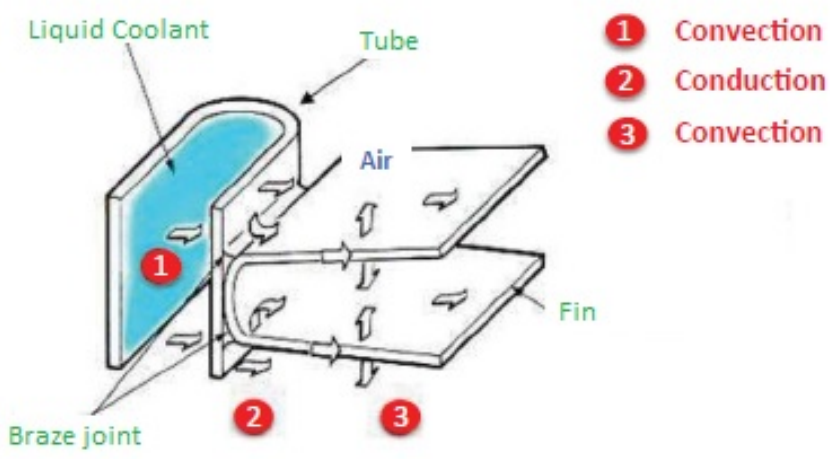

Fig. 1.4. Cooling principle diagram of a heat exchanger [10].

1.3 Brazing

In the 1960s the controlled atmosphere and vacuum brazing were introduced. Before that the mass manufacturing of automotive heat exchangers followed the dip flux brazing. In this process the heat exchanger is dunk inside the flux for the brazing to take place effectively. The main problem of this type of brazing was with the Aluminum surfaces that had residual flux after brazing. Automotive heat exchangers have a large number of components and complex structures. Due to this reason the use of a conventional point welding method which is most commonly used in automotive industry is not preferred widely. Depending on the size of the engines and the stresses induced, the choice may vary between using either a mechanical or a brazed assembly. In the case of cooling radiators, the brazing process is chose because of their dimension and the pressure constraints they must hold in for good performance.

1.3.1 Definition and Principle of Brazing

The brazing consists of the assembly of two metal parts with the aid of a filler metal having a lower melting temperature than the parts to be assembled. During this operation, the filler metal passes into the liquid state and wetts the surfaces to be assembled by capillary action. The base metal does not participate by fusion in the construction of the joint [11], unlike welding there is no fusion of the assembled edges.

The diffusion of the various elements guarantees the metallurgical continuity between the filler metal and the base metal.

Two major brazing techniques are:

Soft Brazing - The melting temperature of the filler metal is less than 450°C. This process uses heavy metals such as tin, lead and zinc.

Strong Brazing - The melting temperature of the filler metal is higher than 450°C. This process uses an aluminum alloy as filler metal. Due to the environmental problems caused by the large-scale use of materials for soft brazing, weak mechanical properties (especially in temperature) and constraints which affect thermal cycling, the strong brazing process is preferred in this application.

1.3.2 Strong Brazing

The high temperatures involved in a strong brazing process impose the use Aluminum alloys with no structural hardening effect under any major modification of the desired properties for the final product. Alloys of series 1XXX, 3XXX and 5XXX appear as excellent candidates. It is similarly to take serious precautions with Al-Mg type alloys of the 5XXX series due to a high reactivity between Magnesium and the use of a brazing flux.

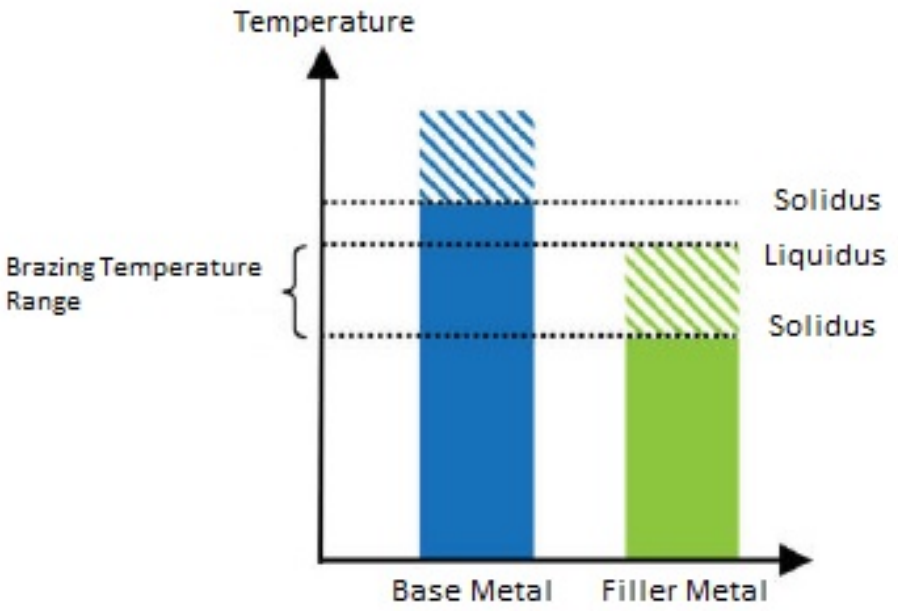

Fig. 1.5. Showing the temperature range for brazing

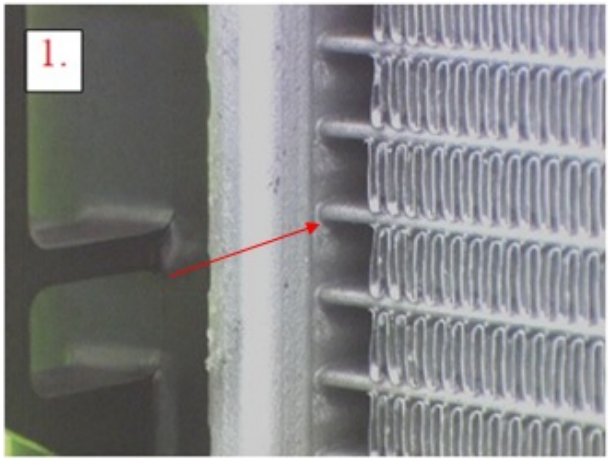

Fig. 1.6. Tube to header joints

1.4 Filler and Braze Flux

The different filler metals that can be used are mainly derived from series 4XXX (Al-Si). The Silicon content of these alloys defines the temperatures to be reached

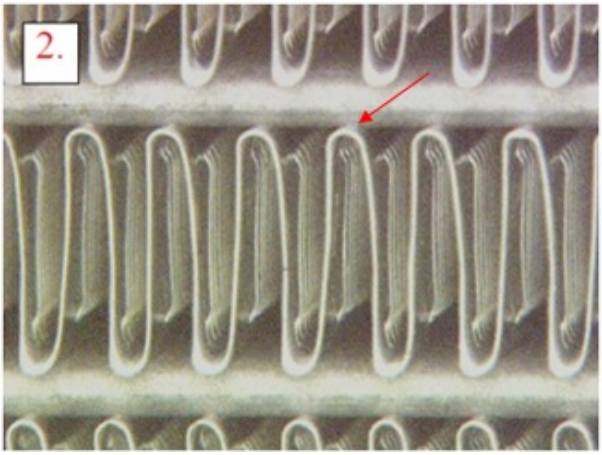

Fig. 1.7. Fin to tube joints

during brazing process. It also highlights the need to use a flux (compound added to the surface of the sheets prior to the brazing step) during the brazing process.

Fluxless brazing is carried out in vacuum furnaces. The flux itself proves to be expensive and adds significant costs to cleaning and maintaining the facilities. The primary role of flux is to remove oxide layer naturally present on the surface of the Aluminum alloys. It also protects the bare metal from re-oxidizing in the furnace. It is expected to lower the filler metals surface tension and promote wetting of the base metal. To allow this action, the flux must have a melting point lower than the brazing temperature. According to Sichen et al., the partial dissolution of Aluminum oxide follows equation (1.1) [12]:

$$Al_2O_3 \longrightarrow AlO_2^- + AlO^+ \tag{1.1}$$

The fluxes currently used are essentially based on chlorides, alkaline fluorides and alkaline-earth metals. The chlorides greatly favors the corrosion by pitting Aluminum, system containing this element must be thoroughly cleaned. This cleaning is added to the cost of installations and makes the process flow itself quite expensive. To overcome these shortcomings vacuum brazing process was developed. This type of brazing does not require flux [13]. This process has the great advantage of being compatible with

the brazing of materials containing a large Magnesium concentration (greater than 1 %). The presence of Magnesium is essential because by diffusing in to the surface it evaporates and breaks the layer of Alumina which covers the parts to be brazed enabling the plating to wet the surface. Moreover, the Magnesium vapor generated also has the advantage of purge the atmosphere of the furnace from residual traces of oxygen and water vapor [14].

Various brazing methods can be used. In this study, the method of brazing under controlled atmosphere with a non-corrosive stream of the Nocolok type developed by Alcan is used.

1.5 NOCOLOK Brazing

Developed at the end of the 1970s by Alcan [15], Nocolok brazing has gradually superseded vacuum brazing [16]. The Nocolok brazing method has the advantage to be able to be used continuously unlike vacuum brazing and importantly at a much lower cost [17, 18]. It consists of brazing in a low-nitrogen atmosphere (-40°C ±10°C) at atmospheric pressure, using a non-corrosive flux KAlF type composed of an optimized mixture of $KAlF_4$ (approximately 75%) and K_2AlF_5 [19]. This mixture is deposited on the surface of the exchangers most often in an aqueous solution (5 to 10% of flux in water) by immersion or sprinkling. The flow remains inactive below 560°C and becomes active at the brazing temperature. The work of Lauzon et al. and Wallis et al. describes the various phase transformations of the compound K_2AlF_5 during the rise in temperature to make it active [20]. It is this compound which converting to K_3AlF_6 will react with $KAlF_4$ and liquefy the mixture at a temperature close to 570°C thus making it possible to remove the oxide layer at the surface before the metal contribution does not establish. At the end of the brazing after the re-solidification of the filler metal, the flux also re-solidifies. The phases involved are assumed to be $KAlF_4$ and K_3AlF_6 [21]. The compound $KAlF_4$, like the compound K_3AlF_6, will preferably be present in the form of colorless platelets [22, 23]. Future

works on of these residues are devoted to interactions with coolant and corrosion phenomena [24, 25]. The impact of flux residues on mechanical strength has never been studied.

Nocolok brazing offers many advantages: non-corrosive flow, no rinsing, low flux consumption and continuous brazing. One of its main limitations is the the inability to braze materials containing more than 0.3% Mg [26,27]. According to Yamaguchi et al. this restriction would be due to the reaction of magnesium with $KAlF_4$ according to reaction (1.2) [28].

$$KAlF_4 + Mg \longrightarrow KAlF_4 + KMgF_3 + K_3AlF_6 \longrightarrow KMgF_3 + K_3AlF_6 \qquad (1.2)$$

This reaction can also prove to be harmful during the brazing process itself and explains the limit of magnesium content set at 1% for Aluminum alloys used. According to Gray et al. [29], the flux residues present on the surface of exchangers after brazing are partially constituted by a K-Mg-F type phase and also even on Aluminum alloys with low magnesium content. Such a reduction reaction of the flow efficiency during brazing leads to a formation of the compound $KMgF_3$ whose melting temperature is 1070°C, thus preventing a good flow of the filler material. In order to avoid this reaction, special flux containing Cesium has been developed. These allow the brazing of material with a concentration of Magnesium up to 0.5% [30]. Another strategy is to prevent the magnesium to diffuse up to the surface by manufacturing alloy sheets not just three layers instead having a 4 or 5 interlayer. The additional layers then play the role of barrier to the diffusion of Magnesium [31, 32].

From an industrial point of view, brazing is carried out in several stages:

1. **Assembly of the components** - The tubes, manifolds and fins are arranged in a frame. This step is usually automated because it requires great precision .This frame allows the contact of the front components for brazing, a spring system prevents the formation of clearances when the metal of background. This step is essential because it forms the base contact for braze joints.

2. **Degreasing** - This step consists of removing the residue of used oil from tubes or fins, as well as any other dust or dirt present on the surface of the components.

Their elimination is necessary for not only brazing, but also to minimize post-brazing corrosion induced by carbon residues. Two degreasing solutions are possible. Degreasing is done mainly by a heat treatment at a temperature around 300°C.

3. **Application of the flux** - This is done mainly by immersion or sprinkling of an aqueous solution containing 5 to 10% flux. In some cases, components may be pre-fluxed before assembly.

4. **Drying** - This step, carried out at approximately 350°C, makes it possible to evaporate the water and to carry out the first transformations of the flux so that it becomes reactive and can remove the oxide layer during brazing.

5. **Brazing** - Performed around 600°C for 5 to 10 minutes, it is during this stage that the filler metal will melt and will be able to form the various braze joints.

6. **Cooling** - In order to solidify the brazing joints, the exchanger passes through a part of the furnace for a cooling of the order of 60°C - 70°C / min.

Fig. 1.8. illustrates the formation of a brazing joint between a tube and fin. In the Fig. 1.8.a, before brazing the laminated structure of the tube is clearly visible and the sacrificial metal layer appears in white and the base metal in brown. The interlayer is brought into contact with the tube in order to allow the formation of the brazing joint. Fig. 1.8.b, shows this same structure after brazing: the joint has formed continuously assembling the tube and the fin together.

1.6 Operating Demands on Cooling Radiators

Heat exchangers are subjected to severe thermo-mechanical constraints and chemical reactions with environments aggressively. Some of them are briefly discussed below:

1.6.1 Corrosion Phenomena

Aluminum is a very reducing metal. The thermodynamic potential of the Al/Al_3^+ is -1.67 V with respect to the normal hydrogen electrode [33]. This makes it a very

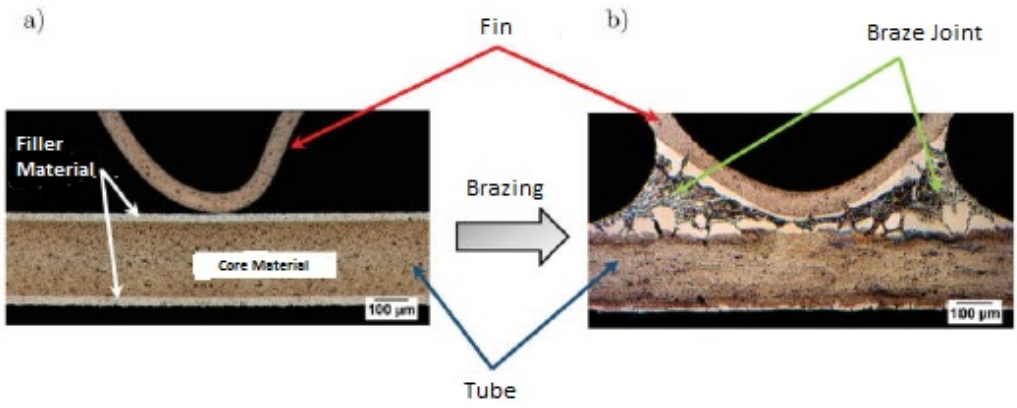

Fig. 1.8. Optical micrographs showing the assembly between a tube and fin a) before brazing and b) after brazing

unstable metal in aqueous solution. Its high reactivity nevertheless leads to spontaneous formation of an oxide film on its surface, even in the air. This limits the phenomena of diffusion and makes possibility of corrosion. This oxide layer however affects the brazing process. Fig. 1.9. shows the diagram of potential - pH balance of Aluminum in water at a temperature of 25°C. This shows that the oxide film is stable in aqueous solution in the pH range included between 4 and 9. Under these conditions, the Aluminum is protected from corrosion.

Heat exchangers, more specifically cooling radiators located in the front of the vehicles are in direct contact with the atmosphere and are usually prone to parameters causing corrosion. Many corrosion mechanisms are likely to interact with the aluminum tubes, which are a key element of the exchangers. Some of the typical types of corrosion occurring is mentioned below:

- Pitting corrosion [34, 35]
- Intergranular corrosion [36]
- Galvanic corrosion [37, 38]

- Corrosion erosion

- Exfoliation corrosion

These are multi-parameter problems for which standardized tests are most often set up in the laboratory [39]. In addition, the constant decrease in thicknesses to reduce the overall weight and material usage needs to be deeply studied to understand the kinetics of deterioration by corrosion. In one of the material configurations studied thereafter, the choice of 7072 Aluminum plating enriched with Zinc has been made to combat the internal corrosion of the tubes. In the material type Al-Mn (series 3XXX), the plating itself acts as a sacrificial anode. Made of a more negative corrosion potential than the Al-Zn alloy and other family of alloys, the plating will corrode preferentially thus prolonging the integrity of the core material.

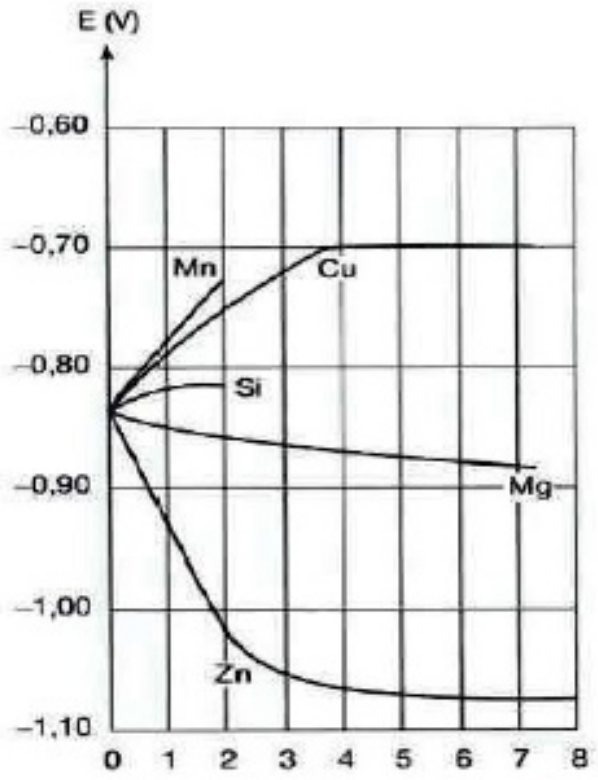

Fig. 1.9. Influence of alloying elements on the corrosion potential of aluminum alloys [40].

Although the corrosion resistance of the Al-Zn plating has been analyzed and quantified [40], its influence on mechanical strength of the cooling radiators has not been published in the literature (to our knowledge).

1.6.2 Thermo-Mechanical Stresses

Origin and Analysis of Thermo-Mechanical Stresses

Different modes of loading are to be taken into account when one wishes to understand the mechanisms of damage to the materials which constitute the various elements of cooling radiators.

Brutal variations in pressure in the loop of the fluid to be cooled and continued sudden changes in the engine speed or the opening of thermostatic valves. This phenomenon is now easily reproducible on a bench in a laboratory through pulsed pressure tests.

Thermal shocks are caused by a sudden and significant change in the temperature. They are caused by the sudden entry of hot coolant into the radiator. In order to quickly operate the engine to an optimum temperature, the coolant does not pass immediately into the radiator. It enters only once a certain temperature has been reached (of the order of 95°C - 110°C.) These variations are induced by the opening of the calorstats, which are equipped valves sensors for measuring the temperature of the engine. Since the components of the radiator are of different geometries and natures, their temperature rise is not homogeneous. Under the effect of heat, they will expand and lengthen. However, the tubes at the ends of the radiator are blocked by the header. As they are thicker and colder, they expand much less quickly (the coolant is not directly in contact with them). Since the end tubes cannot expand with the rest of the tubes, bending phenomena occur at the tube ends as shown in Fig. 1.10. These thermo-mechanical constraints are only transient, once the steady state has been reached; the temperature is substantially the same throughout the exchanger.

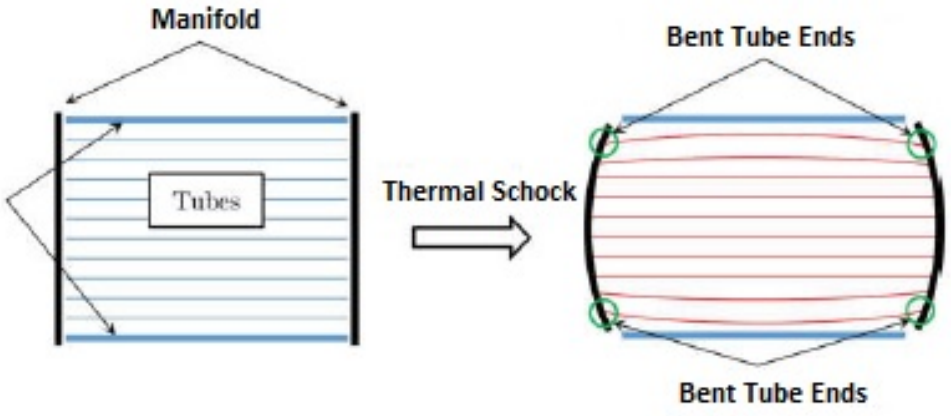

Fig. 1.10. Showing the expansion of a cooling radiator during a thermal shock. The location of stresses occurs at the edges of the end tubes

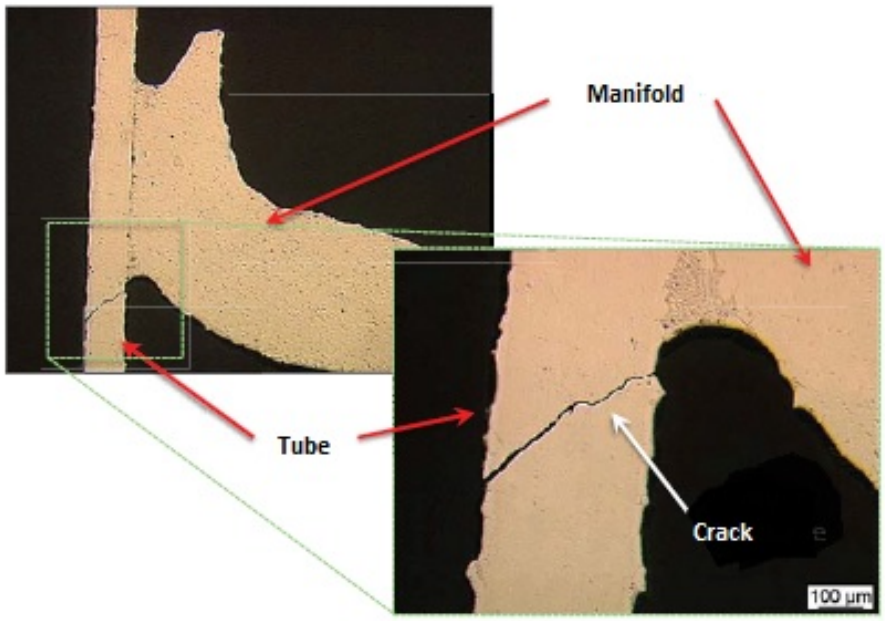

Fig. 1.11. Fatigue crack located at the bottom of the tube, near the braze joint with the manifold in a charge air cooler.

Test benches allow reproducing these different modes of loading in order to test the response to damage to the complete heat exchanger. Local measurements of

temperature and deformation on a test bench in cyclic pressure were thus carried out. Experimental measurement methods able to determine the temperature and stress fields during thermal shock have also been developed [41]. The instrumentation of radiators by strain gauges showed that, contrary to vibration stresses or by pressure variations, thermal shocks cause plastic deformations and are therefore very damaging for the radiator [42].

During the phenomenon of thermal shock, the damage is mostly localized at the bottom of the tube, at the braze joint with the manifold [43]. This translates into cracking of the tubes which no longer ensure the perfect seal required by this type of structure. The tubes mostly concerned are those subject to the greatest variations, i.e. the tubes at the top and bottom ends of the heat exchangers (Fig. 1.10.)

An example of crack is seen in Fig. 1.11 with a tube / manifold brazing joint. It is easy to observe the presence of a crack through the thickness of the tube. It is interesting to note that one end of this crack is near the braze joint.

2. LITERATURE REVIEW

2.1 Microstructure of Pre-Brazed Aluminum Alloys

The alloy 4045 is present on the surface of the base metal in the form of small grains. It consists of an Aluminum matrix containing many particles of globular silicon (Fig. 2.1). According to Marshall et al. and Yoon et al. this globule structure is due to the coalescence of the silicon needles (resulting from the solidification of the eutectic Al-Si) during the various stages of manufacturing of the plated sheet [43, 44]. The very low quantity of iron in the filler metal can give rise to the formation of small precipitates of the type Al_3Fe(Si), α-AlFeSi and β-AlFeSi [45].

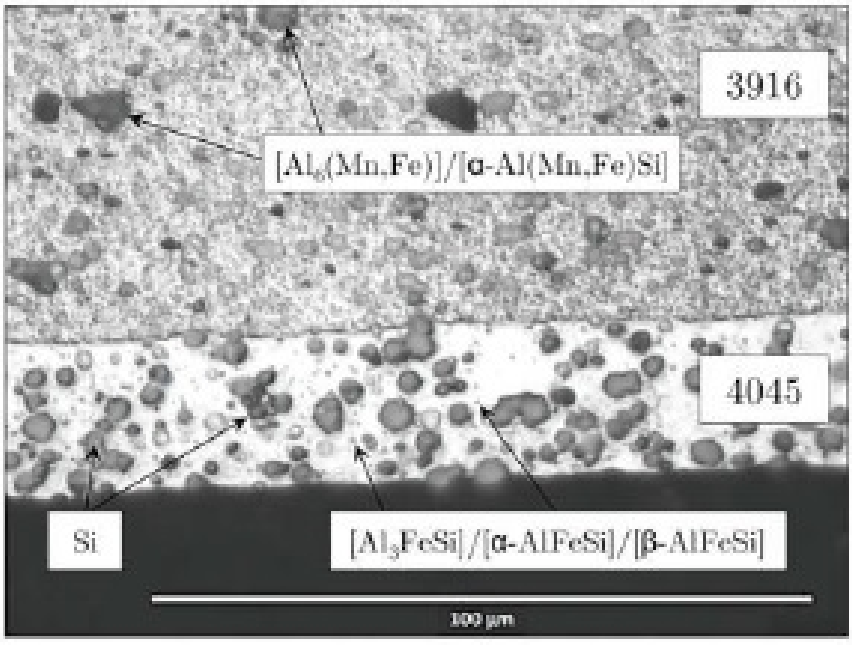

Fig. 2.1. Optical micrography after Keller reagent attack on 4045 and 3916 before brazing showing the different phases present [45]

2.2 Microstructure of the Core

Precipitation phenomena in 3XXX type of alloy were mainly studied for the AA3003 alloy. It has a Manganese composition similar to that of 3916 (between 1.0% and 1.5%) [46] but has a lower concentration of copper: [0.05% 0.2%] compared to [0.5% -1%] for 3916. Iron and Manganese have a low solubility limit in aluminum: 0.052% for a binary alloy Fe-Al and 1.82% for a binary alloy Mn-Al [47]. Given the low solubility of the Manganese in the Al-Mn solution, this is mainly found in dispersoids and intermetallic compounds. Different authors have described the microstructure of the 3XXX alloys (essentially AA3003) as consisting mainly of Manganese-Aluminum dispersants of the α-Al (Mn, Fe) Si and precipitated from Al_6 (Mn, Fe). According to Li et al. as well as Alexander et Al. the latter undergo a partial eutectoid transformation during heat treatments (Mn, Fe) to α-Al (Mn, Fe) Si [48, 49].

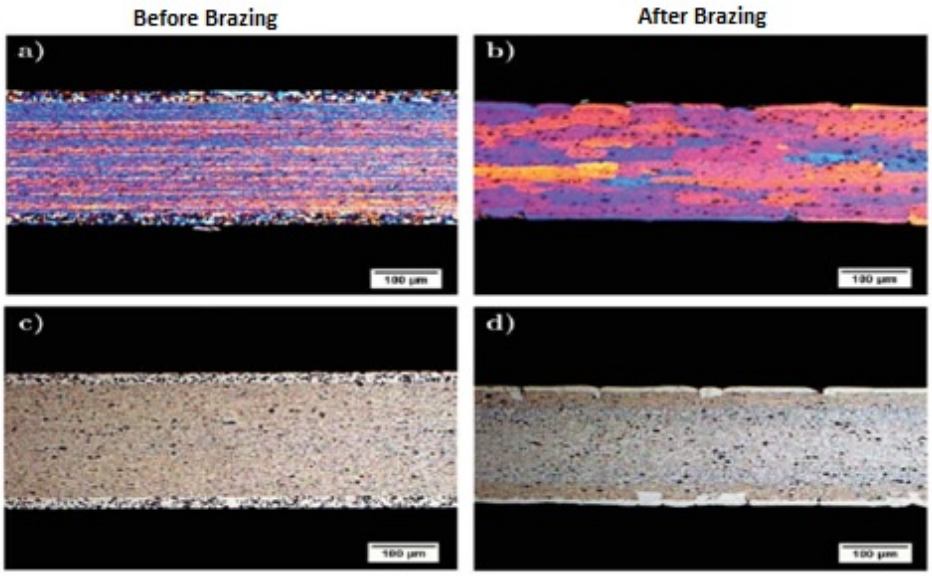

Fig. 2.2. Optical micrographs after anodic oxidation and Keller reagent on a core alloy 3916 coated on both sides with an AA4045 alloy, a) and c) before brazing, b) and d) after brazing [45]

2.3 Microstructure of Aluminum Alloys After Brazing

Recrystallization and Precipitation in the Core

The new grains formed are larger than before brazing, with an average size of the order of 20 μm, ie less than ten grains in the thickness of the sheet, and an average size of the order of 100 - 300 μm in the direction of rolling. Even after recrystallization, the grains texture are elongated in the direction of rolling. This shape is sought and developed within the framework of the alloys in a concern for resistance to corrosion [50].

These alloys, of which 3916 is a part, also rely on of the brazing of a sacrificial zone called "Brown Band" or BBP (Brown Band Phenomena), See Fig. 2.3.a) This area located just below the interface between the residual plating and the core is widely described in the literature [51–53]. This diffusion leads to a reduction in the solubility of the Manganese in solid solution in the inducing core a phenomenon of precipitation [54]. These precipitates (or dispersoids) are small (Fig. 2.3.b), of the order of 30 to 100 nm [55], mostly composed of Aluminum, Manganese, Silicon and trace Iron and are in the cubic form α-AlMnSi. Benedictus et al. have also shown that for alloys of the 3XXX series containing Copper or Magnesium the phases Mg_2Si and τ -AlCuMn also precipitate [56]. According to brazing cycles applied Marshall et al. have shown that silicon diffuses between 40 and 70 μm. This depth of diffusion was evaluated in dependence of brazing time, temperature and diffusion coefficients by Sigli et al. [57]. In the case of an AA3005 alloy plated with an AA4045 alloy, the width of the BDP was estimated at 100 μm for brazing at 595°C. for 5 min. Because of this precipitation, the Al-Mn solid solution of the BDP has its reduced Manganese concentration thus decreasing the corrosion potential of this zone, which favors the lateralization of the corrosion in the BBP [58].

Furthermore, after brazing the primary precipitates Al_6 (Mn, Fe) are still present in the base metal although their concentration has decreased according to the work

of Alexander et al., Li et al. But also from Warmuzek et al. the transformation of the Al_6 (Mn, Fe) phases into intermetallics -Al (Mn, Fe) Si has taken place [59, 60].

With regard to the microstructure of alloy 4045 after its resolidification, two distinct zones can be described: braze joints and "flat areas" away from these joints.

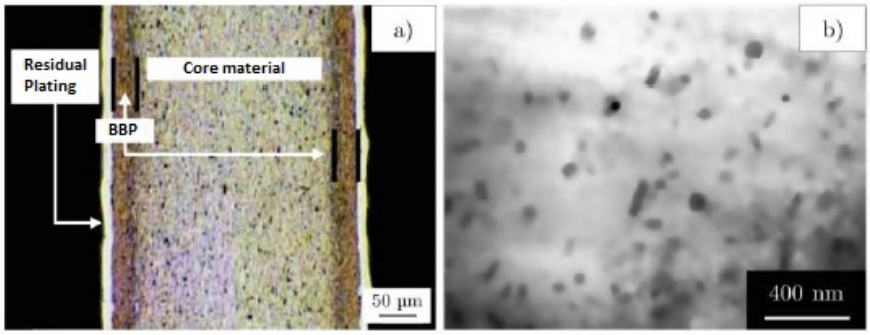

Fig. 2.3. Sheet after brazing consisting of modified alloy 3003 plated on both sides with an AA4343 alloy. a) Optical micrographs after reacting with Keller reagent. The BBP appears in brown and the residual plating in white. b) Micrography obtained in the BBP zone showing dispersoids [61].

2.4 Microstructure Resulting from the Resolidification of the Molten Metal

2.4.1 Formation and Structure of the Brazing Joint

During brazing, the 4XXX alloy moves to a liquid state and forms brazing joints by capillarity between the components in contact. The formation of the joint will depend on the brazing temperature, the distance between the components to be assembled, their geometry, the amount of filler metal available and also the orientation of the exchanger during brazing (gravity playing a role in the distribution of molten metal) [62]. During cooling, the microstructure of the brazing joint corresponds to that observed during a solidification of the Al-Si eutectic. An example of a brazing joint between a tube and fin is given in Fig. 2.4.

Different authors have focused on the microstructural description of the brazing joint. Thus Sekulic et al. were interested in observing and then modeling solidification in the case of a type 3003 core alloy and a 4343 type plating. Particularly the morphology of the dendrites as a function of brazing parameters were studied [63], [64]. The authors have thus shown that, during solidification there is first formation dendrites of solid Aluminum solution followed by the deposition of a eutectic Al-Si aggregate characterized by the presence of silicon wafers. Dehmas et al., and Tierce et al. also described the intermetallics present in the brazing joint [65]. These intermetallic compounds are in the form of α-Al (Mn, Fe) Si needles but also under more complex forms always of type α-Al (Mn, Fe) Si. Manganese and Iron present in the brazing joint result from a phenomenon of partial dissolution of the core during brazing.

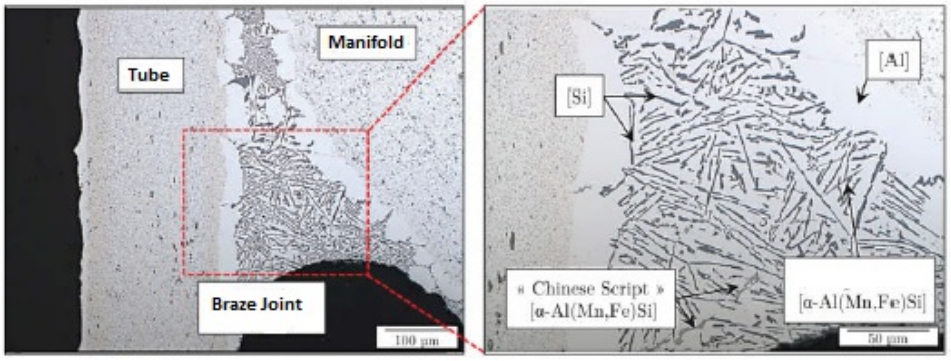

Fig. 2.4. Optical micrography after a Keller reagent attack showing a joint of brazing (alloy 4045) between a tube and a manifold Philipps et al.

Different models have been established based on the minimization of potential energy and have been correlated with experimental data. The authors have shown that distribution of the molten alloy is essentially dictated by the wetting of the core material. The liquid accumulates at the point of contact between the various parts and the seal formed has concave shape. Taking into account the formation of a residual plating film on the surface of the tubes away from the braze joints; Zellmer et

al. have been able to improve their model [66]. Gao et al. correlated the thickness of this residual plating with the formation of braze joints by application of the principle of mass conservation and thickness measurement of residual plating [67].

2.4.2 Microstructure of the AA4045 alloy outside of the braze joints

The 4045 alloy which has not migrated to the brazing joints, forms a thin film of residual on the whole of the planar surfaces. Fig. 2.5 gives the structure of this film. Seen from the surface, Fig. 2.5.a), the film is composed of large Aluminum grains whose size varies from 100 μm to 1 mm separated by regions appearing in black. According to Tierce et al. these regions are called "valleys" corresponding to the grain boundaries of the resolidified plating. The Fig. 2.5.b), suggests that resolidification has begun with the formation of Aluminum grains and that the contraction of the volume left a gap between the grains. At the end of the process, the resulting phases of solidification of the liquid metal residue are deposited therein. The grains consist of a solid solution of Aluminum and the valley is composed of Aluminum, Silicon needles and precipitates the Al-Mn-Fe-Si elements. Precipitates of the same composition are also observed at the surface of the resolidified plating in the middle of the grains suggesting to the authors that these are formed at the beginning of the solidification process and have been pushed towards the surface with the growth of Aluminum grains.

Still in this study, Tierce et al. described the nature of these precipitates and details of the solidification path. By measurements obtained in X-ray dispersive spectroscopy, the authors showed that the various precipitates containing the elements Al-Mn-Fe-Si encountered in the residual plating but also in the braze joints have a cubic crystallographic structure of α-Al type (Mn, Fe) Si with different substitution rates between Manganese and Iron. It should be noted that in addition to these -Al (Mn, Fe) Si type precipitates, intermetallics of δ-AlFeSi types have been identified

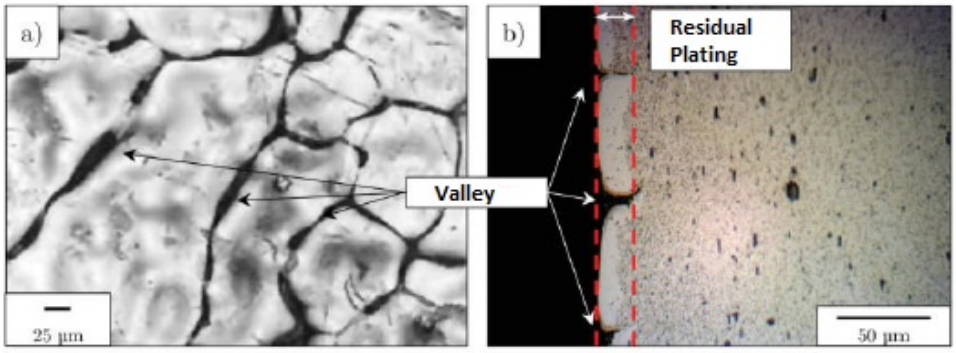

Fig. 2.5. Optical micrographs of the residual plating layer. A) Plating surface residual structure showing the heterogeneous structure of resolidified plating Warmuzek et al. B) Sectional view after Keller attack, the residual plating appears in white, the valleys correspond to the grains

[68, 69]. Although not foreseen by the Al-Si-Mn ternary phase diagram, the authors assume that this phase is stablein the Al-Mn-Fe-Si quaternary diagram.

The nature of the phases being established, the resolidification sequence of the molten plating could be determined by thermodynamic calculations using the CALPHAD method. Using the software Thermocalc, Lacaze et al. determined the resolidification sequence in the brazing joint and in the residual plating. Taking into account the variations in composition in Manganese between these two regions, in particular due to the phenomena of dissolution of the level of the brazing joint, they were able to determine the following sequences:

—In the brazing joint: (Al), (Al) + α-Al (Mn, Fe) Si,

—In the residual plating: (Al), (Al) + Si, (Al) + Si + α-Al (Mn, Fe) Si

The residual plating film thus formed may not be completely uniform. Buteri et al. have observed the formation of residual plating drops during the brazing of test specimens of 3916 plated with an alloy 4045. For these authors, the formation of these drops would be due to the non-use of liquid plating in the creation of braze joints.

From a microstructural viewpoint, the authors have shown that residual plating drops have a structure similar to observed during eutectic Al-Si solidification.

2.5 Interaction between the molten metal and the core

Because of its passage to the liquid state during the brazing step, interactions occur between the liquid 4XXX alloy and the 3XXX core still in the solid state. In the literature, these interactions could be:

- Dissolution: The filler metal in the liquid state statically dissolves the base metal in the solid state with which it is in contact. The higher the temperature, the brazing time and higher the dissolution will be.

- Erosion: Flow of the filler metal in the liquid state on the surface causing a rapid dissolution of the base alloy in the liquid state on which it flows. The driving force of this flow may be gravity or a difference in surface tension.

- Liquid Film Migration: Static reaction during which a solid structure is consumed by a liquid front in motion (and not in convection) that decreases the free energy of the system and leaves behind a solid with a different composition. Unlike dissolution, no dendritic structure is observed.

Several authors have been interested in phenomena occurring at the interface between the filler metal in the liquid state and the solid base metal. According to Nylen et al. partial dissolution of the core material occurs at the accumulation points of the liquid metal [70]. The penetration is then controlled by the degree of hardening of the core material, melting point and the duration of the brazing cycle. After wetting all the free surfaces of the core material, the molten metal preferably moves towards the points of contact between the parts to be assembled. The liquid then enters the core material via its seal network of grains. The diffusion of the silicon from the liquid towards the core leads to a local decrease in the point of melting of the base alloy and thus its dissolution [71].

Kim et al. worked on the evolution of the microstructure as a function of the thickness reduction rate during the cold rolling step [72]. For this purpose, they applied 3003 plated on both sides with a 4045 alloy three reductions of different thickness. These samples were brazed and the obtained microstructure was analyzed. This study shows that the depth of dissolution is proportional to the degree of plastic deformation of the core. Thus for the samples having the rate of reduction of thickness, the dissolution of the core is limited. The grains of the cladding appear to grow epitaxially from the core during cooling. Conversely, a significant dissolution of the samples presenting a low degree of deformation as well as a microstructure which has not grown epitaxially. Two mechanisms for recrystallization of the molten plating thus exist, both controlled by the degree of deformation and which in one case may lead to dissolution of the core. Several limitations can be made to this study. First, the authors performed brazing cycles with a time of maintenance of the order of 30 min against 5 to 10 min for the brazing of an exchanger. A high holding time leads to a greater diffusion of the Silicon and will favor the dissolution phenomena [73].

This point is important because it has been shown on the one hand that the intermediate restoration stage has a very strong influence on the microstructure obtained after brazing and on the other hand that a competition can be between recrystallization and liquid film migration during brazing [74].

The occurrence of liquid film migration in the case of brazed Aluminum alloys is a controversial subject. Some authors have indeed linked the phenomena of dissolution observed during brazing to liquid film migration [75–77]. Liquid film migration occurs in many alloys as a result of temperature as for example in Al-2.07% m Cu [78] or Mo-Ni- (Co-Sn). Rhee et al. show that the diffusion process creates a deformation gradient coherent process that induces formed liquid films to migrate to higher energy areas [79]. For more information on the mechanisms at work in the LFM may refer to the article by Yoon et al. for very detailed on this subject [80]. Woods and Yang worked on brazed alloys of type 3003 clad with an alloy of type 4147.

Dissolution by the mere penetration of liquid grain boundaries that cannot explain the microstructures obtained, as well as the dissolution observed, the authors linked these phenomena to the liquid film migration. By performing thermal treatments processes at different stages of the brazing cycle on specimens having different levels of strain hardening, they have demonstrated that the liquid film migration begins even before the plating based. This migration, which can reach 25 μm is accompanied by epitaxial formation of new grains as well as a magnification of the Silicon particles due to its migration.

At higher temperatures, the authors also showed that the melting of the plating takes place at the plating / core interface. This was explained by the dissemination of the various elements of alloys at the interface locally decreasing the melting point. The liquid thus formed migrates resulting in a significant change in the composition of the base metal in the areas traversed by the film. In the affected area, Manganese, Magnesium, Copper and Iron are collected and pushed forward by the migration of the liquid film leaving behind a zone depleted in these elements but enriched in Silicon (Al-Si solid solution at about 1.5% m Si). The liquid film migration leaves behind it a thick region without any precipitate, separated from the core by a strip of dense intermetallics of the α-Al- (Mn, Fe) -Si type which delimits the final position of the liquid. The Fig. 2.6. illustrates this process. The state before brazing is given on the micrograph Fig. 2.6.a) while Fig. 2.6.b) shows the case after brazing where the liquid film migration did not occur. Fig. 2.6.c) gives the microstructure obtained in the case of a liquid film migration after brazing. The white areas correspond to the affected area and the interface with the core alloy is clearly delimited by a dense band of precipitates. It should be noted that the original interface between the plating and the core can be observed (appearing in the form of a thin dispersoids). The authors assume that the liquid zone becomes quite voluminous to dissolve all the dispersoids.

For Wittebrood, the driving force behind this phenomenon is not the energy of deformation but rather of a residual deformation in the form of dislocations (or of a sub-grain structure) providing the energy required for the movement of the liquid film.

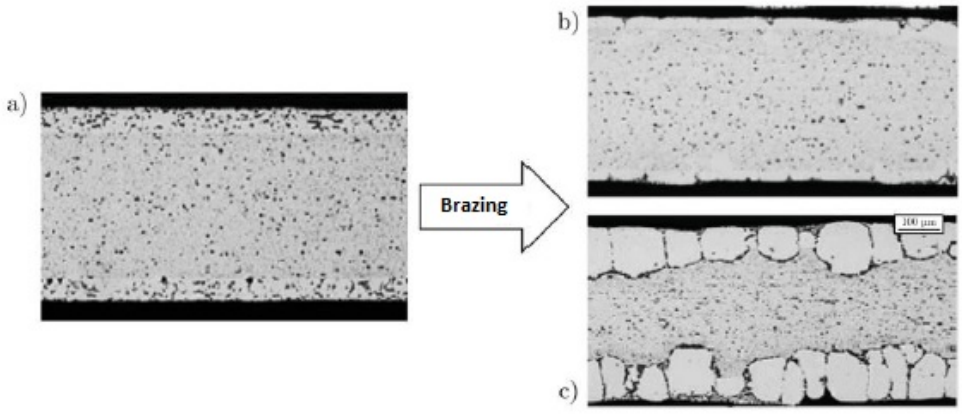

Fig. 2.6. Optical micrographs showing a) material before brazing - b) material After brazing, in the case of a weak interaction between the plating and the core - c) the material after brazing, in the case of a very strong interaction between the plating and the core Nylen et al.

The mechanism at the origin of the liquid film migration is considered to be similar to the recrystallization process in the sense that it is induced by energy stored in the form of dislocation. More precisely, the authors have shown that the reduction of the surface energy between the grains by a liquid film allows the joint to move for a lower dislocation density compared to the system not infiltrated by a liquid film. Moreover, the phenomenon of recrystallization also reduce the density of available dislocations removing at the same time the driving force necessary for the liquid film migration. Thus the liquid film migration and the recrystallization are both in competition for the same energy. If the recrystallization takes place before the appearance of liquid then there will be no liquid film migration.

According to Wittebrood and al. these processes take place simultaneously:

1. Migration of liquid film
2. Dissolution in front of liquid film
3. Re-solidification behind the liquid film
4. Transport of material from the front to the back of the liquid film
5. Transport of liquid from the residual plating to the liquid film

6. Diffusion from the liquid film to the core
7. Diffusion from the core to the liquid film

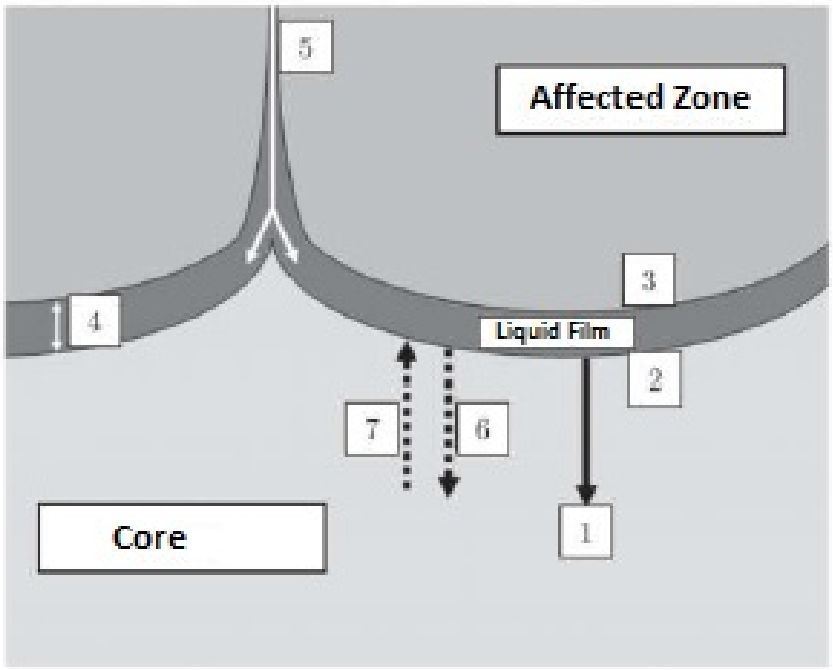

Fig. 2.7. Diagram showing the different processes taking place during the migration of a Liquid film Nayeb-Hashemi et al.

Brazing therefore has a very strong influence on the microstructure and the final composition materials. Many phenomena occur and will change the physical properties of the materials, whether in terms of brazability, corrosion resistance or mechanical properties.

2.6 Fatigue Damage

General Information on Fatigue Damage

Definitions

The definition of fatigue in materials science given by Bathias et al. is a good start into the matter. It is defined as a term which applies changes in properties which can occur in a metallic material due to the repeated applications of stresses or strains, although usually this term specially applies to those changes which lead to cracking or failure [81].

Auguste Wöhler is one of the first to undertake a systematic study of this mode of damage. It was his name given to the curve of endurance which consists in subjecting each specimen to cycles of periodic forces (mostly sinusoidal) of maximum amplitude and constant frequency and to measure the number of cycles at the end of which the rupture occurs:

- At high stress, a zone of oligocyclic plastic fatigue occurs. In this area the break occurs after a relatively small number of cycles and is accompanied with significant plastic deformation.

- At lower stress, an area of fatigue or limited endurance. In this the rupture is reached for a number of cycles which are smaller as the amplitude of constraint is great.

- An endurance zone long regarded as unlimited that it is agreed to call Endurance limit. In fact metallic alloys do not actually have endurance limit which leads to consider a 4th domain.

- An area corresponding to gigacyclic fatigue. In this area the limit of endurance continues to decrease as the number of cycle increases.

The breakage of a part or a test piece by fatigue can be broken down into three parts:

-priming phase corresponding to the appearance of the first microcracks within the material.

- a slow propagation phase where the cracks initiated will grow stably and cycles as a function of the imposed load.

- a phase of sudden propagation leading to rupture when the stress in the section becomes greater than the material breaking stress.

Priming

Experience shows that in general crack initiation results from the appearance of plastic deformation occurring in a finite dimensional domain and generally quite small.

Priming in crystalline metal materials can essentially occur from three ways:

- by irreversible cyclic slip of the dislocations (not very active in industrial metallic materials). The application of a cyclic loading will lead to the appearance of reliefs associated with the formation of localized deformation bands. The formation of these bands in the most active sliding planes leads to the formation of intrusions and extrusions as schematically shown in Fig. 2.8. These bands will then give rise to the formation of stage I microcrack. As can be seen Fig. 2.8.b, stage I microcracks have a size in the order of grain size. From that the microcrack encounters the first grain seal, it bifurcates and then spreads. In a direction perpendicular to that of the greatest main stress (stage II). The appearance of slip bands is generally early; it is the formation of microfissures in these bands which is particularly slow. Microcrack formation and stage I can occupy up to 40 to 90% of the lifetime of the test pieces commonly used to determine the W*ö*hler curve. Note that in the case of gigacyclic fatigue is no longer microcracks but micro-defects that control lifespan.

- from micro-heterogeneities present in the microstructure such as: porosities, inclusions, intermetallic particles, precipitates, grain boundaries. Crack initiation

from these heterogeneities results from incompatibility of elastic and / or plastic deformation.

- from the geometrical particularities of the part such as: notches, fillets, holes. In this case the crack initiation results from a local concentration of constraints.

2.7 Propagation

The propagation of cracks is generally described in the context of linear mechanics, which is based on an analytical solution of the stresses in the vicinity of the crack tip and the introduction of a stress intensity factor.

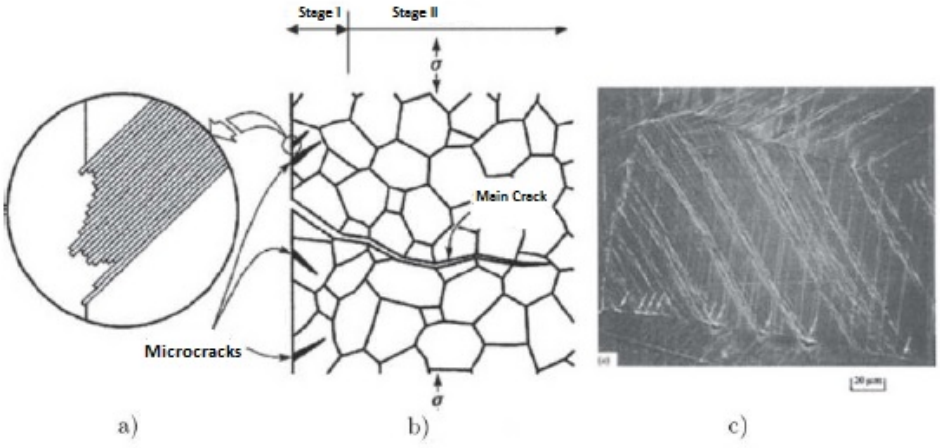

Fig. 2.8. a) Priming of microcracks and formation of intrusions and extrusions to the free surface (sectional view); b) formation of a main crack from microcracks; c) aspects of intrusions and extrusions and cracks from stage I to surface of a copper fatigue specimen [82].

2.8 Mechanical Properties of the Brazing Joint

Before brazing, during the rolling and homogenization stages prior to manufacture of the plated sheet, several authors have shown that silicon diffuses from plating to the alloy of the core. The silicon dissolves in the matrix of the alloy 3XXX forming a

solid solution [83]. According to Zhao et al., although having a weak curing effect by solid solution, the silicon would increase the work hardening considerably for values of deformation less than 10% [84]. The hardness tests carried out by Liu et al. on a billet of 3003 alloy plated with 4045 alloy by continuous casting show that the latter is harder than 3003. Moreover, due to the diffusion of silicon and Manganese at the interface between the 3003 and the 4045, diffusion zone of the order of 30 μm is formed and is also harder than the core [85].

Since the brazing process has a very great influence on the microstructure, certain authors have been interested in the influence of this process on the mechanical properties. Nayeb et al. in their study, seek to determine the impact of brazing time on strength of the joint between two parts in 3003 brazed by an alloy 4047. The authors found that the increase in brazing time results in a decrease in the limit of breaking of the brazing joint. On the other hand, based on tests carried out on a 3003 alloy, the authors show that the increase in brazing time does not limit to rupture of the core. According to Nayeb et al., the reduction of the rupture in the brazing is linked to the reduction of the eutectic present in the joint and the brazing time (silicon diffusion) relates to the formation of porosity (related to the dissolution of the base material) in case of long brazing times (greater than 10 min). In case of short brazing (less than 10 min) the tensile tests show that the test pieces break in the core and not at the brazing joint. This result shows that the area affected by brazing is harder than the core [86].

Edo et al. have characterized the monotonic and cyclic mechanical properties of the brazing. They assumed that the brazing joint had a composition close to filler metal and thus used an AA4045 alloy. By melting this alloy, and by playing on the parameters of solidification the authors obtained different structures of joints having fine, medium or large Si particles. The fatigue tests carried out on these different configurations show that the finer the particles in the brazing joint the higher were the fatigue properties (Fig. 2.9.). The authors attribute this result to fragile character of large particles that promote rapid initiation and propagation of cracks in the joint.

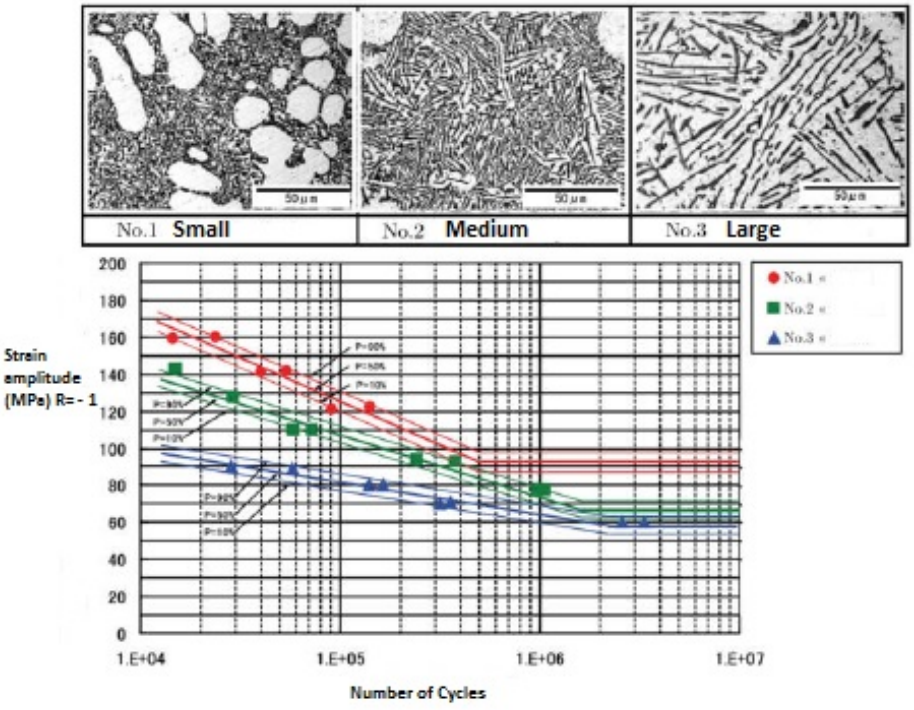

Fig. 2.9. Effect of microstructure on Wöhler fatigue curves for Brazing having a fine, medium and large particle size [87].

Yaguchi et al. and Fujii et al. have been interested in the evolution of the cell structures of dislocations induced in an alloy 3003 by a cyclic loading of tensile-compression [88–90]. These authors have tried to establish a link between the dislocations and the macroscopic lifetime of the alloys studied. They pointed out that the structure of dislocations is dependent on the amplitude in stress and the number of cycles. At high amplitude, dislocation cells are formed and the walls of the cells become increasingly thin as the fatigue deformation progresses. The break occurs for a very small cell thickness and almost constant. In the end, a good correlation between the thickness of the dislocation cells and the lifetime of the test pieces has been found.

2.9 Fatigue and Damage Mechanisms

Apart from the work of Yaguchi et al. and Fujii et al. there are few studies on the fatigue of industrial Aluminum alloys used in the field of automotive heat exchangers from a macro and microscopic point of view. The alloys of the 3XXX series, which have relatively low mechanical properties have been the subject of fewer studies than other structural hardening alloys commonly used. By comparing the mechanical properties of an AA3004 alloy with alloys of different series, it appears that unlike all the others, AA3004 has a fatigue endurance limit higher than its yield strength [91].

Kim et al. studied the effect of brazing on the microstructure as well as on the mechanical properties of an alloy 3005 plated on one of its faces with 4343 and on the other with a sacrificial plating 7072. The authors performed temperature fatigue tests before and after brazing on test pieces having a thickness of 0.4 mm. Before brazing, data could be obtained in both the low and high number of cycles, whereas after brazing only long lifetimes (greater than 50,000 cycles) could be measured. For tests carried out at a very high level of stress (close to the breaking limit), premature rupture is observed for the brazed test specimens. In addition, a degradation of the fatigue strength is generally observed after brazing. The authors attribute this degradation in the surface state of the brazed material. During brazing the recrystallization crevasses between the surface grains (similar to the valleys evoked by Tierce Et al.), which would reduce the mechanical and fatigue properties. However, the authors give no more precision as to the initiation and propagation of the cracks.

Yao et al. carried out fatigue tests with deformation imposed on 3005 alloy plated and having simply undergone the heat treatment corresponding to the brazing cycle to room temperature, 75°C and 180°C. It appears that the lifetime of the plated specimens is shorter than that of the non-plated with strong deformations. This difference tends to disappear for small deformations. According to the authors, the eutectic zones of residual plating appear to be preferred priming zones in fatigue.

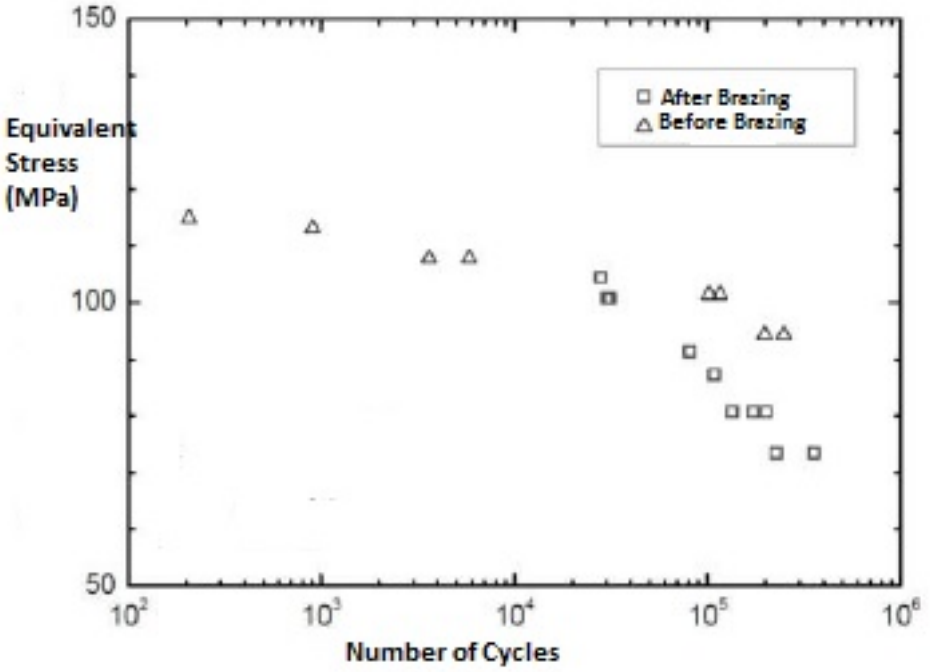

Fig. 2.10. Fatigue tests performed on an AA3005 alloy before and after brazing [92]

Cracks propagate from these fragile areas in the residual plating and then into the core, which would reduce the fatigue life of the plated materials. Finally, this work deals with the influence of the temperature on the fatigue properties and show the reduction of the lifetime when the temperature increases (from ambient to 180°C) for an equivalent level of deformation. Thus the fatigue properties are similar at different temperatures. For the authors, this result would seem to indicate that the mechanisms of damage do not change with at least in a range of 20°C to 180°C.

This issue is precisely the theme of a recent work of Kahl et al. on the tensile, fatigue and creep characteristics of aluminum alloys for heat exchangers with temperatures ranging from ambient to 300°C. The primary aim of the authors were to compensate for the lack of existing data by identifying trends in order to predict the behavior of materials at a temperature where very little data are currently available. After carrying out a brazing treatment on their test pieces, Kahl et al. studied 5 materials having different compositions (different core or plating). A very good cor-

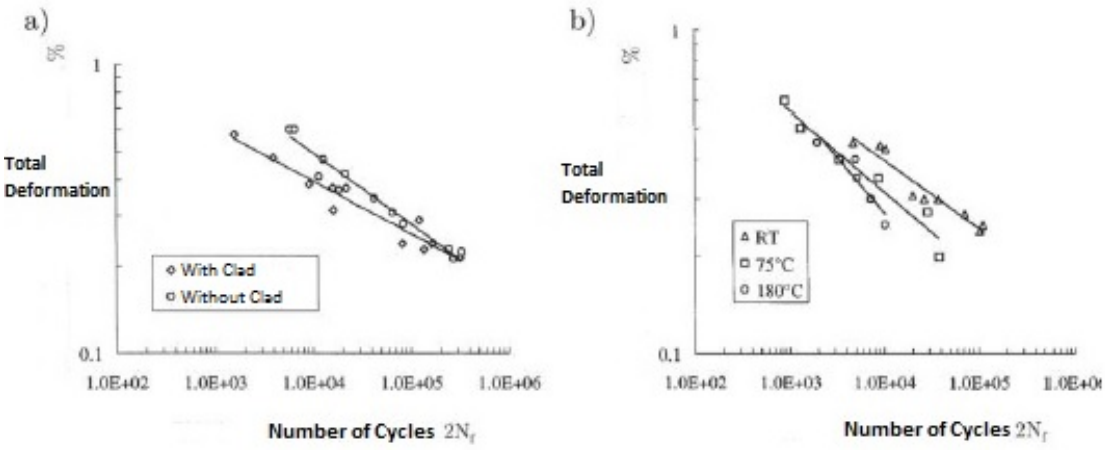

Fig. 2.11. Fatigue curves in total deformation imposed as a function of the number of cycles at a frequency of 0.5 Hz, with a triangular signal and a strain ratio greater than 0 showing a) the influence of 7% AA4104 plating on a 2.5mm thick AA3005 alloy and b) the influence of temperature for a two-sided AA3005 alloy with an alloy AA4343 at 7% (total thickness 3.2mm) [93].

relation between the breaking limit and the lifetime at 105 cycles was found. However, the authors insist that this is a trend and case of a rule: at a given temperature a material having the highest breaking point will not necessarily have the best properties of resistance to fatigue or creep. To overcome this first result, Kahl et al. used the Bergstrm model which allows accounting for true strain curve for an AA3003 alloy [94]. After modification, they were able to successfully calculate and predict interpolated traction curves at different temperatures. Regarding the influence of temperature on the fatigue strength, Fig. 2.12. gives the behavior of an AA3003 alloy plated on both sides by an AA4343 after brazing.

The fatigue strength decreases with the increase in temperature and very few points were obtained for the small number of cycles, which corroborates the results of Kim et al. The authors also note that for fatigue tests at a temperature not exceeding 100°C, almost all of the fatigue specimens broke from sliding bands located on the edge of the test pieces. Furthermore, it is the priming time that dictates fatigue life

and thus result of Buteri et al. and Kahl et al. were unable to observe cracks in the propagation course, this phase being very short. Nevertheless some rare cracks have been observed on the polished section of the specimens.

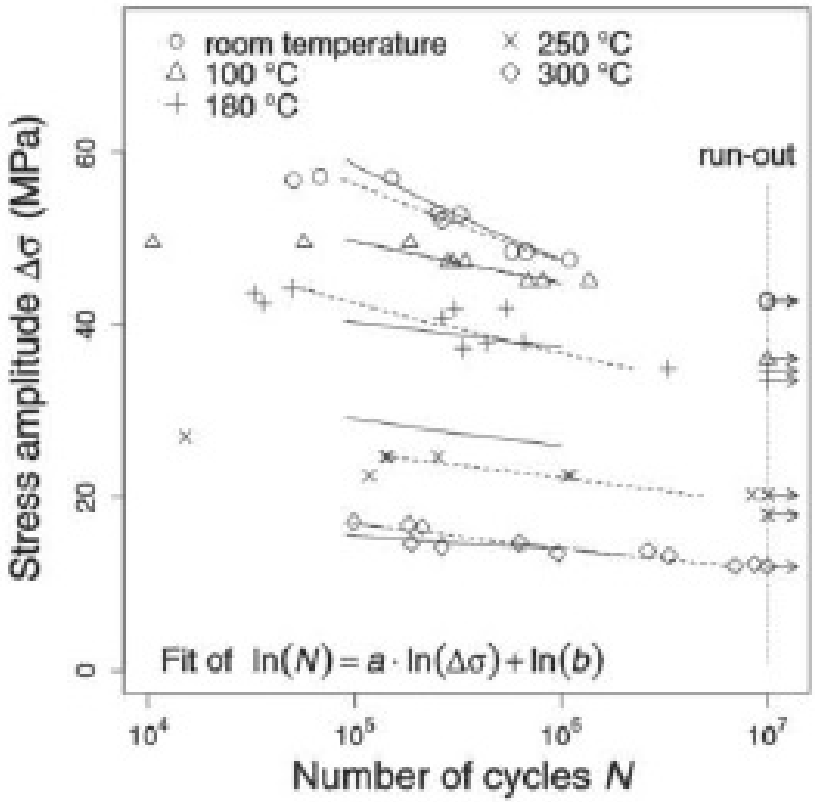

Fig. 2.12. Fatigue curves at different temperatures with constant stress amplitude for AA3003 alloy plated on both sides with AA4343 (10%) after brazing (thickness 0.4mm, R = 0.1, f = 30Hz, and sinusoidal signal) by Kahl et al.

Fig. 2.12 also shows a change in behavior with the increase in temperature. For the authors, the fatigue strength is diminished due to the appearance of a creep deformation at a temperature of between 100°C and 180°C. To prove it Kahl et al. showed that during tests at ambient temperature a high elongation is observed during the first cycle and then decreases from the 4th cycle once the maximum stress is reached.

By performing creep tests and otherwise plotting the lifetime as a function of the temperature, Kahl et al. showed finally that the creep reduces the fatigue strength from a temperature between 100°C and 180°C and that for a higher temperature at 200°C creep seems to dominate the lifetime during a fatigue test. A. Butri was able to show that whatever the material configuration, the phase initiation occurs from microstructural surface heterogeneities present on the plating 4045 induced by the brazing method. Indeed, during a mechanical stress of the tensile type, it appears that the eutectic Al-Si type microstructure constituted by phases (Al (Fe, Mn) Si and silicon needles) is particularly sensitive to the stress levels at the surface of the specimens, which is in agreement with the observations of Yao et al. These different particles located mainly in the level of the grain boundaries, but also at the heart of larger surface heterogeneities are broken in very large numbers when the level of constraint reached increases.

Once the crack is initiated, Buteri et al. have identified three distinct sub-phases during propagation from the observation of fractures. These phases are summarized in Fig. 2.13 a).

- The first corresponds to the stable intragranular propagation phase of the fatigue crack first in the thickness and then in the transverse direction long perpendicular to the direction of stress, whatever the material configuration.

- The second phase called mixed propagation, corresponds to an area in which the speed of the fatigue crack increases significantly. This zone is then characterized by the presence of increasingly distant fatigue striae. Finally a 90° rotation of the fatigue striae is observed translating a rupture.

- The third and last phase of propagation corresponds to the sudden rupture. This phase is characterized by a rupture facies oriented at 45° with respect to the axis of solicitation.

Using correlation images A. Butri has shown that the propagation phase of the crack represents at best only 10% of the lifetime of the specimen as shown in Fig. 2.13

b). The fatigue life of these materials appears to be thus governed by the initiation of cracks.

Finally, tests carried out on specimens of the exchanger type made it possible to corroborate the mechanisms of initiation and propagation of fatigue cracks observed on specimens.

A significant drop in overall service life is observed in the case of tests carried out on pieces of exchangers with equivalent applied stress. This fall is directly attributable to the design of the structure and the stress concentration generated at the tube / manifold brazing joint. The zone of failure of the test pieces of the exchanger types is therefore similar to that observed on complete radiators.

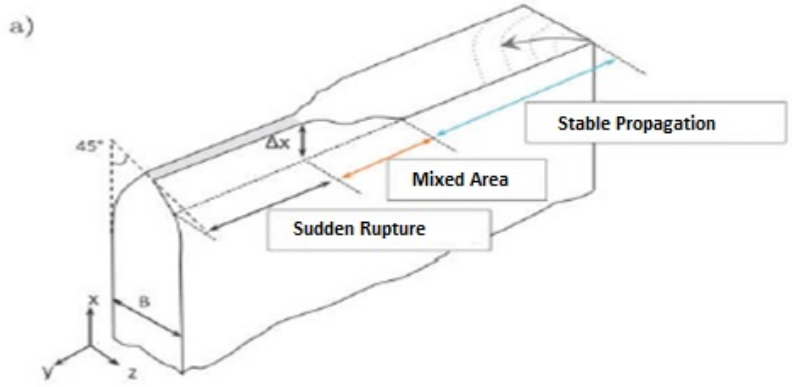

Fig. 2.13. a) Diagram of a rupture facies representing the three phases of the propagation Identified. b) Graph from the correlation data of digital images plotting the deformation in accordance with the standardized lifetime of 4045/3916/4045 alloys after Brazing, tested at ambient temperature with constant stress amplitude at a frequency of 10Hz (sinusoidal signal). The propagation of the crack occurs in the last moments of the lifetime. Buteri et al.

3. TEST MATERIALS AND EXPERIMENTAL METHODS

In this work, in order to study the mechanical properties and damage occurring in the materials used in the brazed cooling radiators, it is necessary first of all to precisely characterize the mechanical properties of these materials. On the basis of these results, the phases of crack initiation and propagation could be analyzed by the mechanisms of damage. This chapter presents the structures, chemical properties and manufacturing of the materials studied and their preparation for test specimens. After a brief description of the mechanical tests and the characterization techniques the methods of monitoring the damage mechanisms put in place are described.

3.1 Materials

The brazing of the heat exchangers requires the use of plated materials comprising, on the one hand, the filler metal and, on the other hand, the core alloy. An additional "interlayer" layer can be added to play a sacrificial role with respect to corrosion. The following parts present the general characteristics as well as the method of manufacturing and for brazing the materials used in this work.

3.2 Structure and Composition of the Subjects Studied

The Fig. 3.1. presents schematically the structures that are the subject of this study. They are all composed of the same core alloy type, 3XXX have a thickness range between 0.2 and 0.4 mm before brazing. They differ from their plating on the air side clad and the coolant side clad.

Table 3.1.
Alloy designations and chemical composition of Aluminum Alloys. (% material by weight, rest of material is Aluminum).

Alloy Designation	Silicon	Iron	Copper	Manganese	Magnesium	Zinc	Titanium	Zirconium
3003	0.6	0.7	0.05 - 0.20	1.0 - 1.5	0	0.1	0	0
3119	0.9	0.7	0.7	1.8	0.03	0.1	0.2	0
4045	9.0 - 11.0	0.6	0.1	0.05	0.03	0.1	0.1	0
7072	0.7		0.1	0.1	0.1	0.8 - 1.3	0	0
3Z23	0.3	0.3	0.6	1.7	0.03	0.05	0.2	0.05
YB-18	0.3	0.7	0.2-0.4	0.6-1.0	0.02	0.1	0.25	0.05
3Z22	0.5	0.5	0.6	1.7	0.03	0.05	0.2	0.05

The standard material used for the manufacture of cooling radiators is symmetrical and is composed of each side of 4045 plating, each representing 10% of the total thickness (Fig. 3.1.a)).

The other (Fig. 3.1.b)) is composed of similar layers and is symmetric. But instead of having a 10% of the total thickness 4045 plating on both sides, the internal clad or the coolant side is plated with 10% of the total thickness of 7072. The 7072 clad is added to improve the corrosion resistance of the alloy. It has added Zn to it that improves the corrosion properties.

The chemical composition of the alloys used is given in Table 3.1. All these materials are manufactured with varying thickness of laminated sheets with a metallurgical state H24 (partially annealed, half hard) and H14 (strain hardened only, half hard).

3.3 Manufacturing Process

These multi-layer structures are obtained by the use of the different rolling method shown in Fig. 3.2 . Several passes are necessary in order to obtain the thickness and the mechanical properties while respecting the integrity of the material. The rolling process may be categorized into three distinct stages:

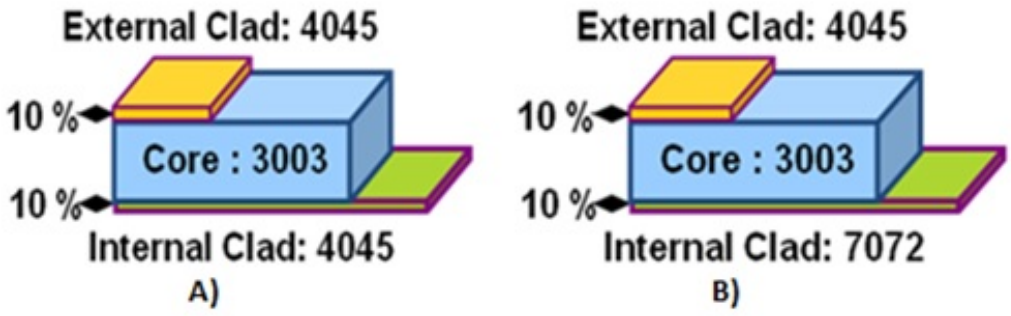

Fig. 3.1. Schematic View of the Materials Studied A) Standard material B) Added corrosion resistance material.

Stage 1: In the first stage, the alloys are warmed up in order to bring them to the rolling temperature and relieve the residual stresses. Then in the second the clad and core materials are sandwiched and are hot-rolled to the desired final thicknesses.
Stage 2: The different ingots are assembled by spot welding in the form of a sandwich according to the desired structure and then hot-rolled to a final thickness.
Stage 3: In this stage a thickness reduction by cold rolling is done to obtain the desired value of thickness. The material is then sheared to the desired width and wound as a coil.

Finally, a restoration heat treatment is carried out in order to restore the mechanical properties of the material and to reach the required metallurgical state. This state allows ideal shaping in the case of cooling radiator tubes.

This process was applied to the material used for studying and having undergone a simple rolling process.

3.4 Brazing and Preparation of Test Specimens

In this study no actual braze joints are formed. The specimens are passed through the conditions at which the actual braze joints are expected to occur. But in this study all of the specimens have no contacts with any metals and no braze joints are

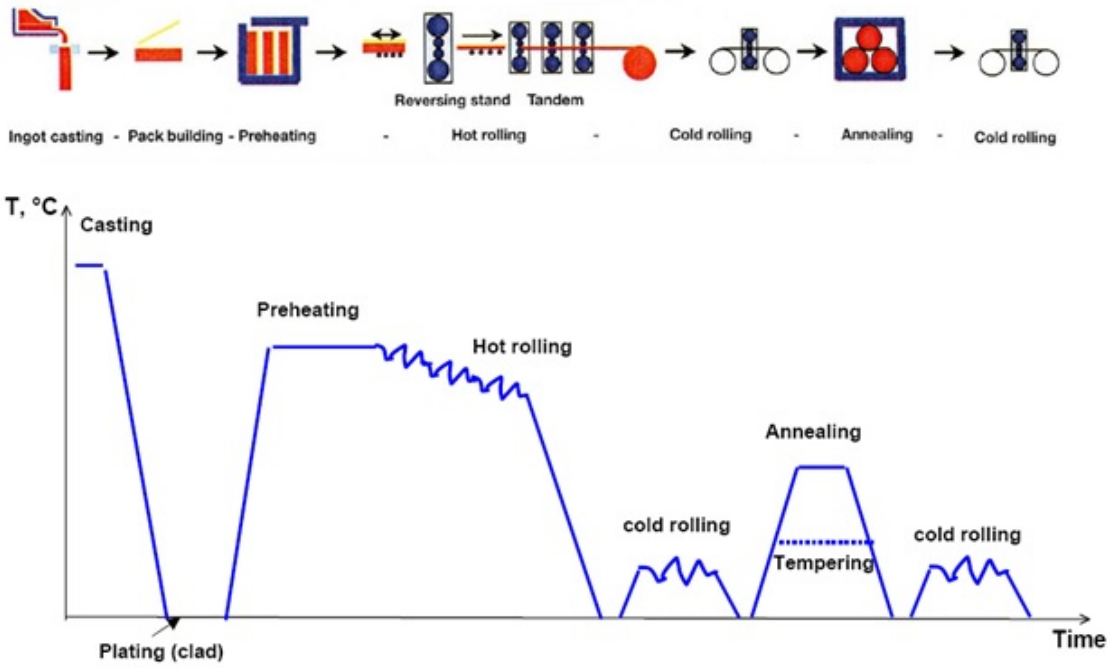

Fig. 3.2. Schematic View of the Manufacturing of the Material Studied.

formed as they are not part of the study. So no braze, after braze and after re-braze conditions in these tests mean,

Braze - The test sample is directly tested without passing any braze conditions.

After Braze - The test sample is passed through the conditions of brazing without forming any braze joints.

After Re-braze - The test sample is passed through the conditions of brazing without forming any braze joints, let cool at room temperature for up to 3 hours, pass again through the conditions of brazing without forming any braze joints.

It has been previously mentioned that the brazing process has a very strong impact on the microstructure as well as on the surface condition. Since the materials are delivered in the H24 or H14 state, it is necessary to carry out a heat treatment similar to a Nocolok flux brazing in order to obtain a microstructure and mechanical properties representative of those of a brazed exchanger tube material.

This procedure is adapted to test samples to study mechanical properties are described below and summarized.

- The sample materials are cut from the coil roll. Sampling of the material is done by the shears in rectangular pieces of 21 inches approximately. The samples are loaded to the sample test apparatus. The apparatus is designed to hold 5 such samples at a time.

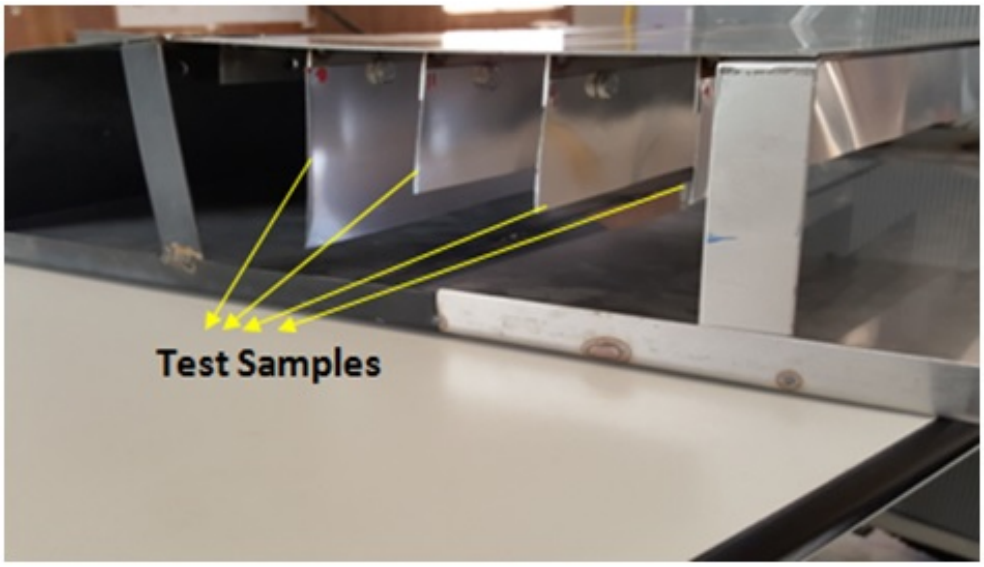

Fig. 3.3. Sample Preparation Test Apparatus

The test sample apparatus with samples are sent through the furnace to simulate exactly the brazing process that the radiator as a whole part would go through.

- Thermal degreasing of the samples is achieved by heat treatment at 250°C.

- A drying step prior to brazing is carried out in order to remove any trace of moisture from the application of the flow.

- As a next step application of the flux by sprinkling on both sides to 5g / m^2.

- The brazing sample is connected to a data logger to verify the temperature time profile for every set of the samples run.

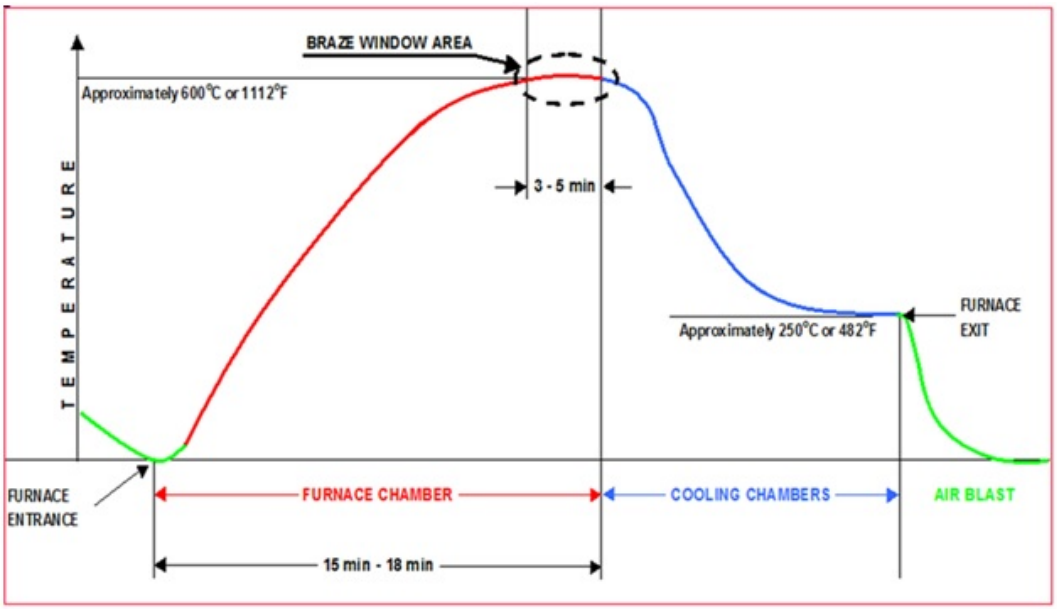

Fig. 3.4. Graph explaining the time of the sample run through the furnace for brazing with respect to temperature.

Fig. 3.5. Sample test apparatus with data logger loaded at the start of the furnace.

The samples collected at the end of the furnace are let cool down for up to 3 hours before they are removed from the apparatus. Once when they are cooled, they were taken to prepare the specimens per requirements and guidelines of ASTM E8 [95].

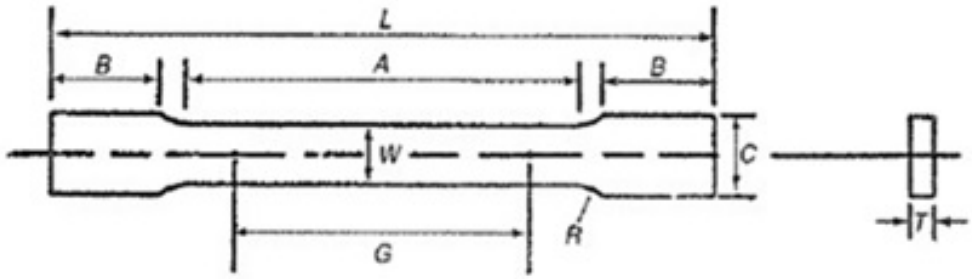

Fig. 3.6. Representation of standard dimensions for test specimen.

Table 3.2.
Standard Specifications of Test Specimen

Parameters	**Standard Dimension (in)**
G, Gauge Length	2.00 ± 0.005
W, Width	0.500 ± 0.010
R, Radius of Fillet	0.5
L, Overall Length	8.00
A, Length of Reduced Section	2.25
B, Length of Grip Section	2.00
C, Width of Grip Section	0.75

The specimen is prepared with the help of a tool that is set designed and made to match the above mentioned standard dimensions. The sample is placed in to the tool and machined to get exact same standard dimensions.

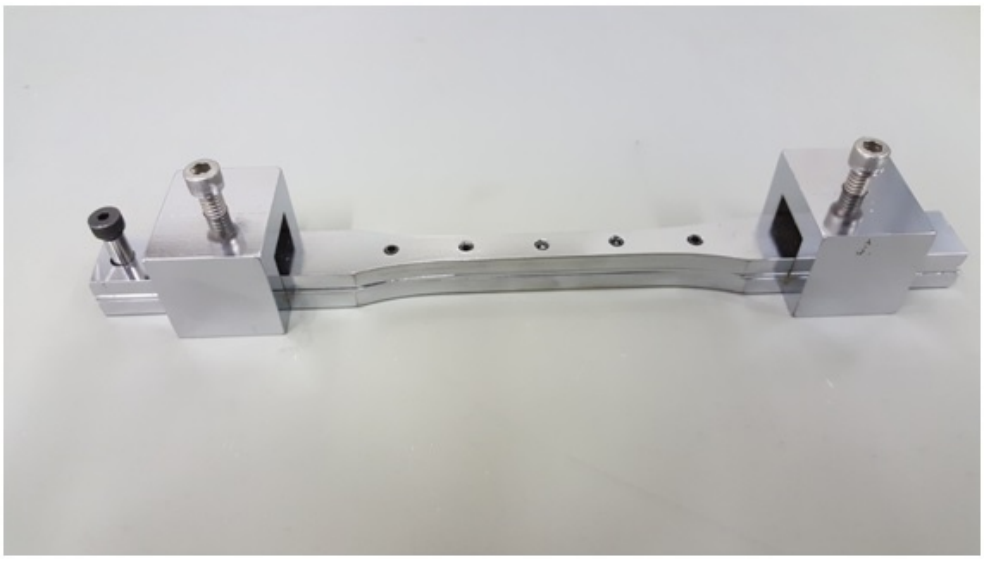

Fig. 3.7. Standard tool used to prepare the test specimen

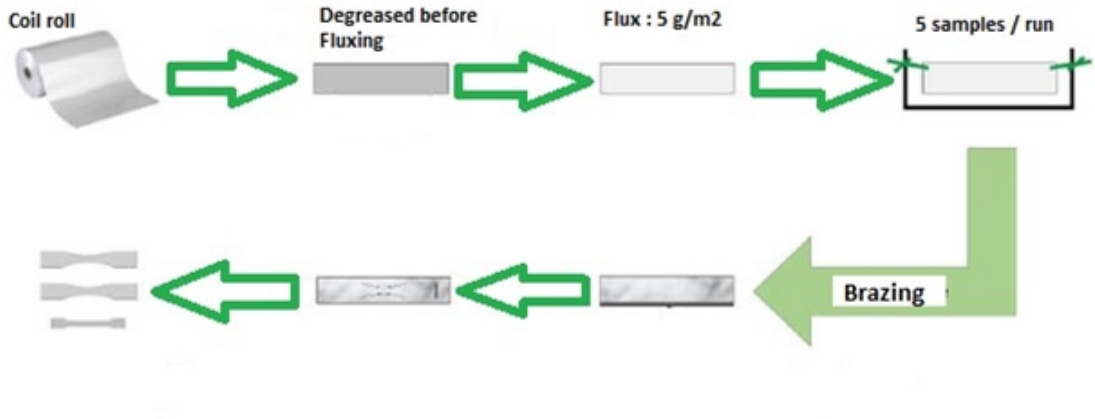

Fig. 3.8. Schematic representation of the steps required to prepare the test specimens

3.5 Mechanical Tests

Tensile tests are performed for a few reasons. The after effects of the tests are utilized as a part of choosing materials for applications. These properties as often as possible are incorporated into material determinations to guarantee quality. They are

frequently are measured amid improvement of new materials and procedures, so that diverse materials and procedures can be looked at. They are utilized to anticipate the conduct of a material under different types of loading.

Tensile testing method is chosen to determine the behavior of materials under uniaxial tension loading. Load - elongation data are used to determine elastic limit, modulus of elasticity, proportional limit, reduction in area, tensile strength and yield strength.

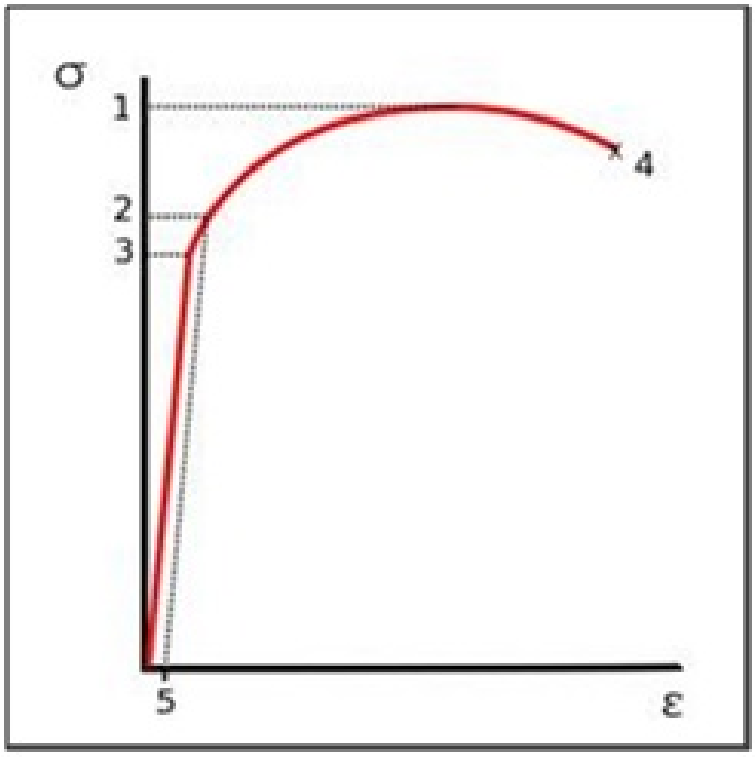

Fig. 3.9. Typical Stress vs. Strain curve of Aluminum

Where,

1. Ultimate Strength
2. Yield strength
3. Proportional Limit Stress
4. Rupture
5. Offset Strain (typically 0.002).

Tensile Tests

The tensile tests were carried out on a MTS Alliance RT/50 machine from the Metallurgy laboratory of Valeo, equipped with a 30kN force cell and laser extensometers. Before each test, the thickness and the width of each of the specimens were precisely measured. These measures were repeated three times and averaged to calculate the initial section of each specimen. At the grip, a pre-load of 1 MPa was applied to the test piece and the test was launched at a strain rate of 0.0025 s-1 controlled by an extensometric system.

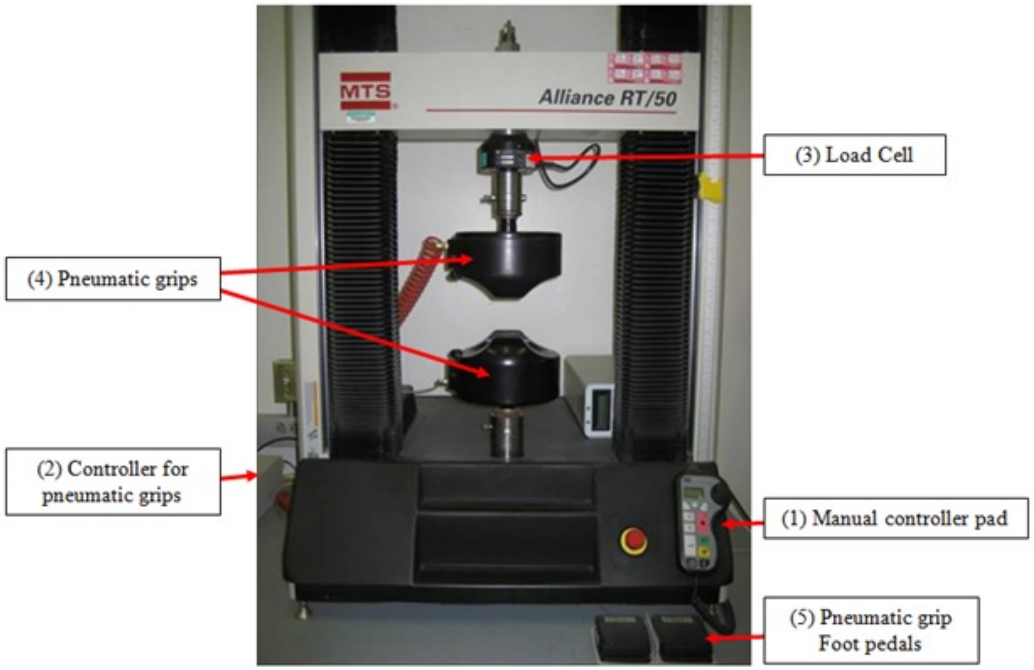

Fig. 3.10. Schematic representation of test equipment.

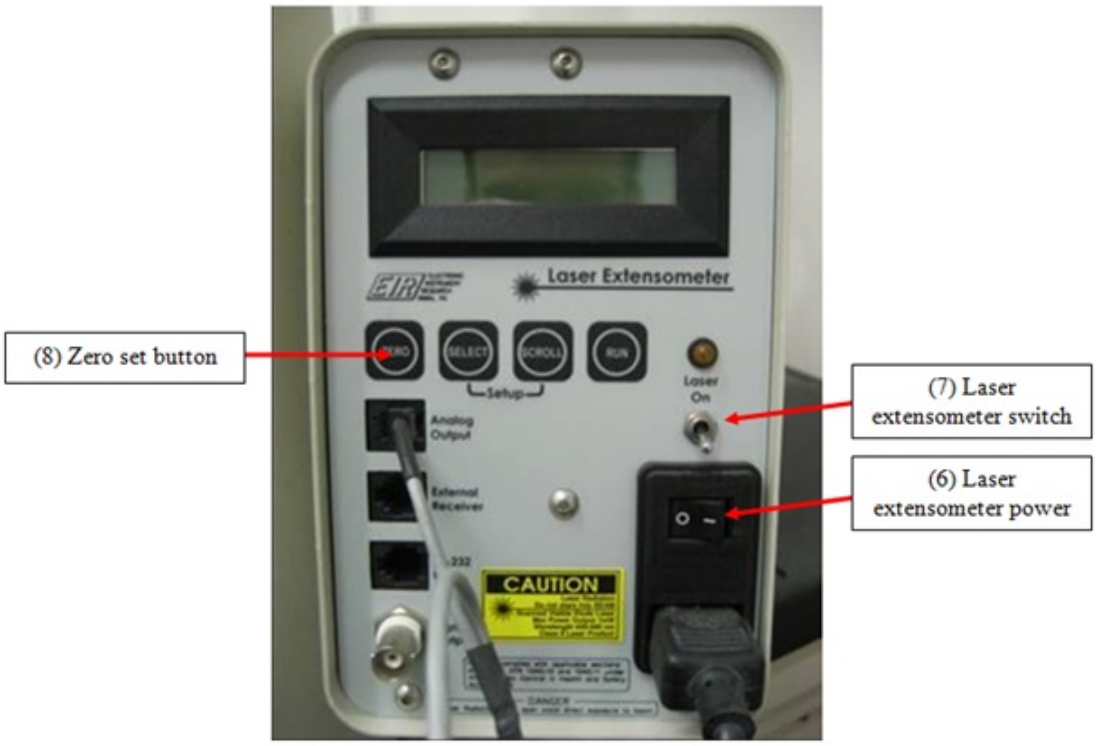

Fig. 3.11. Laser Extensometer used for testing specimens.

Test Procedure

- The power is turned on the MTS manual hand held controller pad (1) as well as the laser extensometer (6).

- The controller for pneumatic grips (2) is checked and air pressure is adjusted to appropriate value for given specimen. The correct load cell (3) 30 KN load cell is made ensured.

- For elongation and strain calculation, the retro-reflective film is installed on the test specimen at the appropriate gage length in accordance with laser extensometer manual and ASTM guidelines (usually 2 inches).

- On the MTS computer, the MTS software is started.

- Using the hand held controller pad (1) and pneumatic grip foot pedals (5) the test specimen in pneumatic grips (4) is installed.

Fig. 3.12. Retro-reflective film (2 inches wide) installed on to every specimen.

- The laser extensometer (7) is switched on and the laser beam is aligned correctly to read the retro-reflective film on the test specimen as per the laser extensometer guidelines. After recording the gage length reading on the laser extensometer, the laser extensometer (8) is zeroed out.

- The information on the test page is reviewed. The load cell and strain gage channels are made online and the values are reset around the zero values.

- The gage length, specimen cross-section dimensions are fed to the system. After appropriate values are entered test is begun.

- When the specimen fails, the test stops. The laser extensometer is turned off using the laser extensometer control pad (7).

- The fractured specimen is removed using pneumatic grip foot pedal (5).

For each specimen, the total number of measurements was 3. Therefore for each alloy 5 specimens were prepared to test.

4. RESULTS AND DISCUSSION

First of all, it is necessary to recall the initial problem encountered in the automotive heat exchanger to determine the mechanisms of failure and damage of brazed structures of the heat exchanger type in order to better understand the reasons of anticipated cracking of the tubes during the operation. Indeed, the real blocking point as a direct consequence of the cracking of a tube is the leak causing the heat exchanger unusable.

In the framework to determine the mechanical properties of tube materials of automotive radiators an experimental study was conducted on ten different tube materials with varying thickness and material composition were subject to test conditions to study their mechanical properties. Table. 4.1 shows the design of experiments used for this study.

The tests were conducted on every type of material for before brazing, after brazing and after re-brazing conditions. For every material, 3 specimens for each case -before braze, after braze and after re-braze were made from the samples and the average of the results are presented. The tests were conducted on these materials as mentioned in the previous chapters. The results are presented below and are discussed.

Table 4.1.
Design of Experiments

Trial	Material	Condition	Thickness	Clad	Hardness
1	A	No Braze	0.23 mm	4045/7072	H24
2		Braze			
3		Re-Braze			
4		No Braze			
5		Braze			
6		Re-Braze			
7		No Braze			
8		Braze			
9		Re-Braze			
10	B	No Braze	0.35 mm	4045/4045	H24
11		Braze			
12		Re-Braze			
13		No Braze			
14		Braze			
15		Re-Braze			
16		No Braze			
17		Braze			
18		Re-Braze			
19	C	No Braze	0.27 mm	4045/4045	H24
20		Braze			
21		Re-Braze			
22		No Braze			
23		Braze			
24		Re-Braze			
25		No Braze			
26		Braze			
27		Re-Braze			

Table 4.2.
Design of Experiments (Continued)

Trial	Material	Condition	Thickness	Clad	Hardness
28	D	No Braze	0.26 mm	4045/7072	H24
29		Braze			
30		Re-Braze			
31		No Braze			
32		Braze			
33		Re-Braze			
34		No Braze			
35		Braze			
36		Re-Braze			
37	E	No Braze	0.4 mm	4045/7072	H24
38		Braze			
39		Re-Braze			
40		No Braze			
41		Braze			
42		Re-Braze			
43		No Braze			
44		Braze			
45		Re-Braze			
46	F	No Braze	0.23 mm	4045/7072	H24
47		Braze			
48		Re-Braze			
49		No Braze			
50		Braze			
51		Re-Braze			
52		No Braze			
53		Braze			
54		Re-Braze			

Table 4.3.
Design of Experiments (Continued)

Trial	Material	Condition	Thickness	Clad	Hardness
55	G	No Braze	0.2 mm	4045/7072	H24
56		Braze			
57		Re-Braze			
58		No Braze			
59		Braze			
60		Re-Braze			
61		No Braze			
62		Braze			
63		Re-Braze			
64	H	No Braze	0.25 mm	4045/7072	H24
65		Braze			
66		Re-Braze			
67		No Braze			
68		Braze			
69		Re-Braze			
70		No Braze			
71		Braze			
72		Re-Braze			
73	I	No Braze	0.35 mm	4045/7072	H24
74		Braze			
75		Re-Braze			
76		No Braze			
77		Braze			
78		Re-Braze			
79		No Braze			
80		Braze			
81		Re-Braze			

Table 4.4.
Design of Experiments (Continued).

Trial	**Material**	**Condition**	**Thickness**	**Clad**	**Hardness**
82	J	No Braze	0.21 mm	4045/7072	H24
83		Braze			
84		Re-Braze			
85		No Braze			
86		Braze			
87		Re-Braze			
88		No Braze			
89		Braze			
90		Re-Braze			

Table 4.5.
Test Material Characterization.

Material Type	**Thickness (mm)**	**Clad (side1/air)**	**Clad (side2/coolant)**	**Hardness**
A	0.23	4045	7072	H24
B	0.35	4045	4045	H24
C	0.27	4045	4045	H24
D	0.26	4045	7072	H24
E	0.4	4045	7072	H24
F	0.23	4045	7072	H24
G	0.2	4045	7072	H14
H	0.25	4045	7072	H24
I	0.35	4045	7072	H24
J	0.21	4045	7072	H14

Table 4.6.
Material A

Property	**Before Braze**	**After Braze**	**After Re- Braze**	**Units**
Width	12.3	12.2	12.2	mm
Thickness	0.23	0.22	0.22	mm
Ultimate Tensile Strength	180	143	152	MPa
Yield Strength	160	55	50	MPa
Elongation at Break	8.0	10.3	18.5	%

Table 4.7.
Material B

Property	**Before Braze**	**After Braze**	**After Re- Braze**	**Units**
Width	12.3	12.3	12.3	mm
Thickness	0.35	0.34	0.32	mm
Ultimate Tensile Strength	194.5	147.5	153.5	MPa
Yield Strength	160	55	53.5	MPa
Elongation at Break	8.9	14.4	16.6	%

Table 4.8.
Material C

Property	**Before Braze**	**After Braze**	**After Re- Braze**	**Units**
Width	12.3	12.3	12.3	mm
Thickness	0.27	0.26	0.26	mm
Ultimate Tensile Strength	174	137.5	152	MPa
Yield Strength	156	56	60	MPa
Elongation at Break	3.0	9.0	15.3	%

Table 4.9.
Material D

Property	**Before Braze**	**After Braze**	**After Re- Braze**	**Units**
Width	12.3	12.3	12.3	mm
Thickness	0.26	0.26	0.25	mm
Ultimate Tensile Strength	180	149.5	155	MPa
Yield Strength	161	59.5	52	MPa
Elongation at Break	7.1	12.5	14.3	%

Table 4.10.
Material E

Property	**Before Braze**	**After Braze**	**After Re- Braze**	**Units**
Width	12.3	12.3	12.3	mm
Thickness	0.4	0.4	0.4	mm
Ultimate Tensile Strength	185	149	140	MPa
Yield Strength	147.5	58.6	54.5	MPa
Elongation at Break	16.3	15.5	17.5	%

Table 4.11.
Material F

Property	**Before Braze**	**After Braze**	**After Re- Braze**	**Units**
Width	12.3	12.3	12.3	mm
Thickness	0.23	0.23	0.23	mm
Ultimate Tensile Strength	176.8	131.1	134.2	MPa
Yield Strength	152.5	47.4	48.8	MPa
Elongation at Break	18.7	17.6	24.1	%

Table 4.12.
Material G

Property	**Before Braze**	**After Braze**	**After Re- Braze**	**Units**
Width	12.3	12.3	12.3	mm
Thickness	0.2	0.2	0.2	mm
Ultimate Tensile Strength	155.1	116.6	115.8	MPa
Yield Strength	146.9	46.2	44.8	MPa
Elongation at Break	4.8	24.3	28.6	%

Table 4.13.
Material H

Property	**Before Braze**	**After Braze**	**After Re- Braze**	**Units**
Width	12.3	12.3	12.3	mm
Thickness	0.25	0.25	0.25	mm
Ultimate Tensile Strength	184.1	149.6	140.7	MPa
Yield Strength	147.5	58.6	54.5	MPa
Elongation at Break	16.3	15.5	17.5	%

Table 4.14.
Material I

Property	**Before Braze**	**After Braze**	**After Re- Braze**	**Units**
Width	12.3	12.3	12.3	mm
Thickness	0.35	0.35	0.35	mm
Ultimate Tensile Strength	193.3	142	130.3	MPa
Yield Strength	173.6	58	47.6	MPa
Elongation at Break	16.3	20	19.7	%

Table 4.15.
Material J

Property	**Before Braze**	**After Braze**	**After Re- Braze**	**Units**
Width	12.3	12.3	12.3	mm
Thickness	0.21	0.21	0.21	mm
Ultimate Tensile Strength	155.4	107.5	115.5	MPa
Yield Strength	141.3	38.9	42.1	MPa
Elongation at Break	8.6	22.6	22.4	%

From the results it is clear that the brazing process has effects in degrading the tensile properties of the material. After the material is gone through the brazing process, the plastic deformation starts to occur at much lower stress levels than the material when before brazing and which is expected to occur. In order to evaluate the materials and their performance when they are re-brazed it is important to look in to their mechanical properties. With the yield strength being slightly higher or similar in the after re-braze materials while compared with the after braze materials, it is evident that there is not much impact on the plasticity and elasticity of the materials. With slightly higher yield strength it is known that the elastic nature of the material is relatively little higher in the re-brazed material. Irrespective of the varying composition of the materials and the thickness of the test materials being different in all the cases, the trend in the properties studied do not have any significant effect. So it is evident the tube materials tested with the alloy interlayer combination considered in this study does not show a lot of variation in the properties tested between after brazed and after re-brazed conditions.

The brazing conditions are decisive; they will condition the final microstructure of the materials as well as their surface condition. For all the materials of this study, during brazing they initially elongate and the flattened core grains recrystallize and form larger grains.

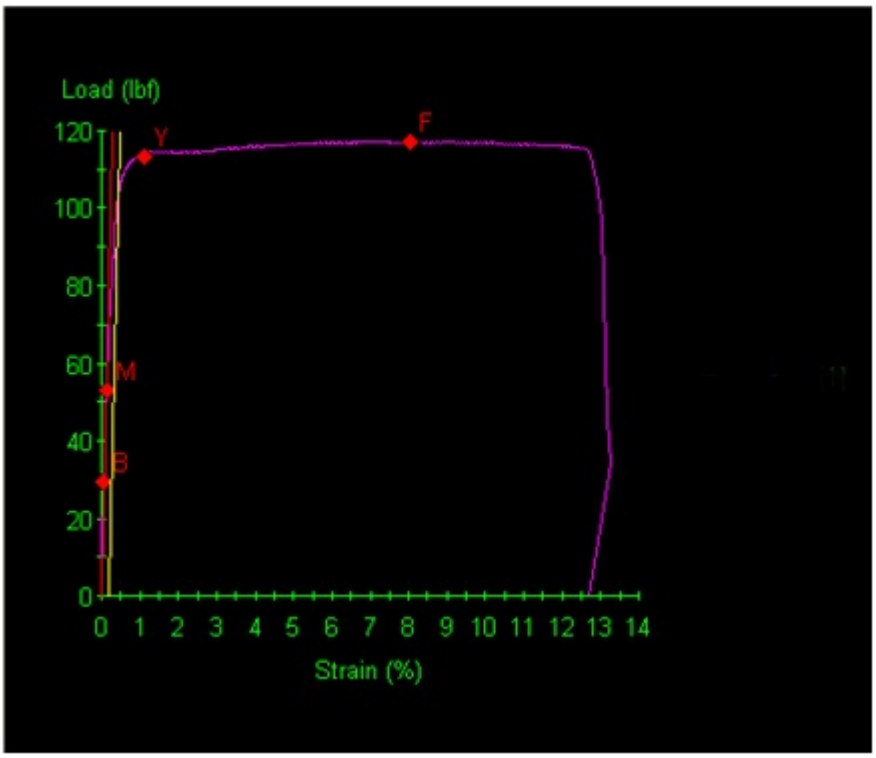

Fig. 4.1. Stress vs Strain curve of test sample material A before brazing. (Young's modulus = 65 GPa)

Most importantly there were not sufficient studies conducted on re-braze conditions. It is convincing that not much in depth understanding of this condition has been analyzed, because it is expected that the process is complete with the first set of braze operation. There are a lot of studies carried out on improving the existing brazing conditions and operations versus going in depth understanding of the re-brazing process. But in real time manufacturing environment the product fails to meet the product validation conditions and there could be many constraints constituting the cause. They are re-brazed under same first braze operating conditions and most of the times pass the product validation. But the product validation was originally based of the first braze process and there could be hidden conditions occurring in the material while going through the re-braze process causing it to pass the product validation but potentially fail at operating conditions. In order to understand the

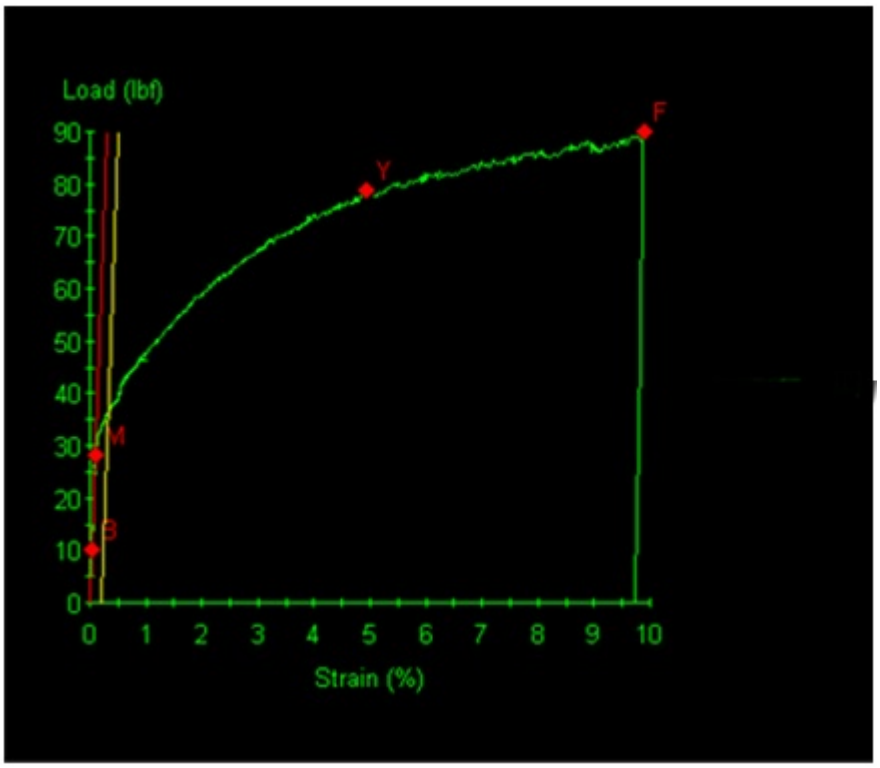

Fig. 4.2. Stress vs Strain curve of test sample material A after brazing. (Young's modulus = 49 GPa)

changes occurring during the re-braze process, the condition re-braze was included in this study. There could be two potential ways to handle this problem. The first one could be a in depth study about the microstructural changes during this operation and analyze their mechanical properties. The second one could be an optimization on the re-braze operational process to specifically handle the second braze condition without having much effects on their expected behavior for successful operation (if there are any).

In materials tested, the 4045 plating on the surface melts when the temperature reaches 577°C. The silicon contained in the clad diffuses towards the core causing the reduction of the core melting temperature. This allows the plating (liquid) to penetrate the core and causes it to dissolve, especially at the level of the grain boundaries. The interlayer at 3003 present in the alloy recrystallizes with the core and does

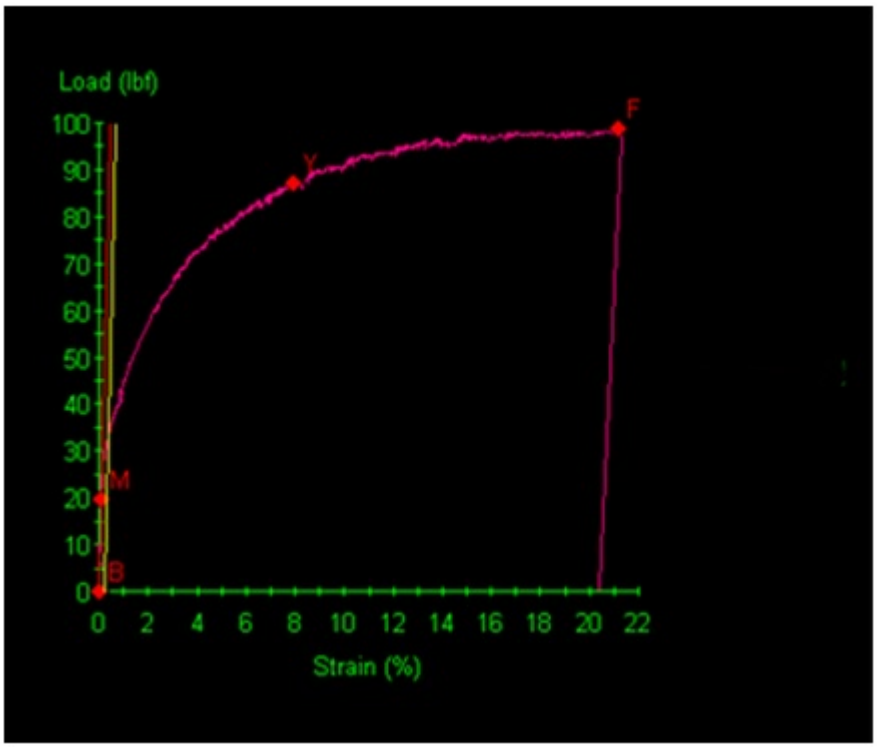

Fig. 4.3. Stress vs Strain curve of test sample material A after re-brazing. (Young's modulus = 32 GPa)

not prevent penetration of the plating into the core. At the end of the brazing, the grains of the materials at the solid / liquid interface begin to grow. The grains thus formed have no crystalline discontinuity between the core and the residual plating. The latter has no dispersoid and has hardness greater than that of the core.

The brazing process causes a recrystallization of the material which results in the formation of a coarse microstructure showing only a few grains in the thickness typically from 5 to 10 grains. The thickness of the material will have considerable effect on the strength properties of the alloy. But in this case where the properties are compared between the braze alloy and the re-braze alloy there are no significant effect on the parameters tested, other than previously mentioned effects. The effect of grain size on strength properties has been studied by many authors for brazing process. The strength properties is expected to decreases with increasing grain size in the thickness.

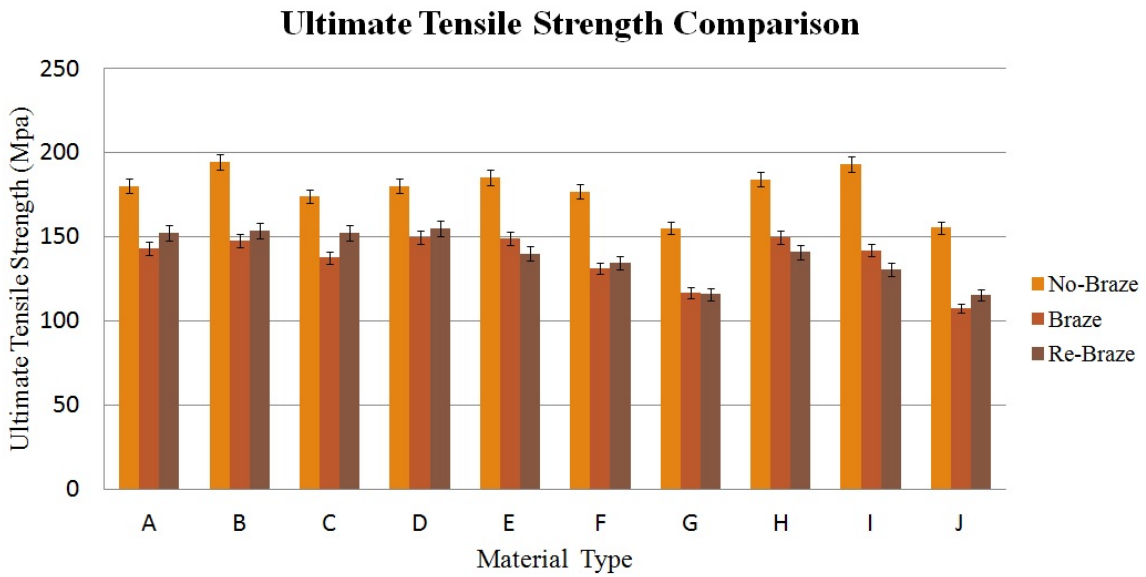

Fig. 4.4. Graphical representation of Ultimate Tensile Strength comparison between the test materials.

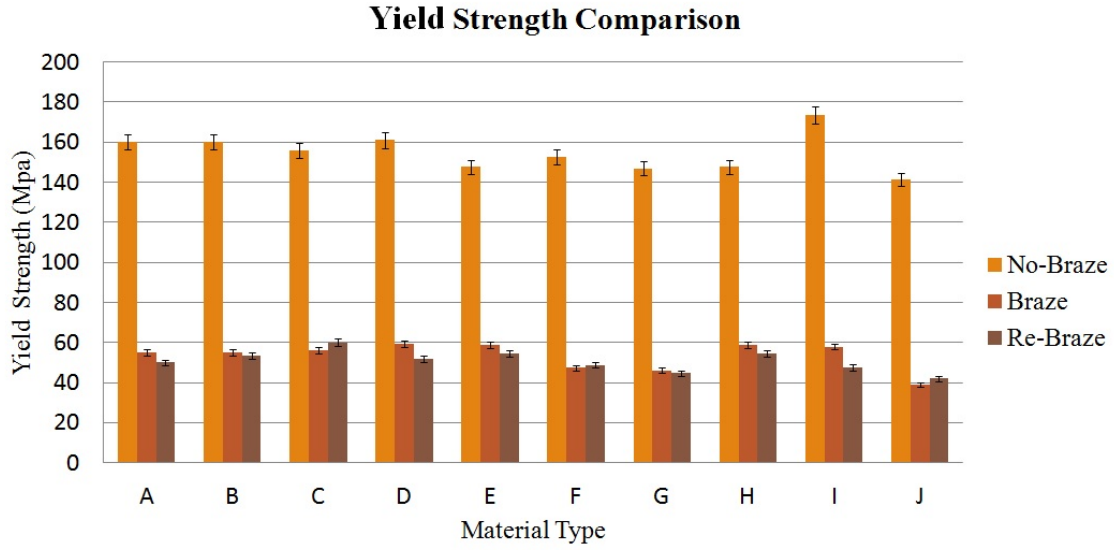

Fig. 4.5. Graphical representation of Yield Strength comparison between the test materials.

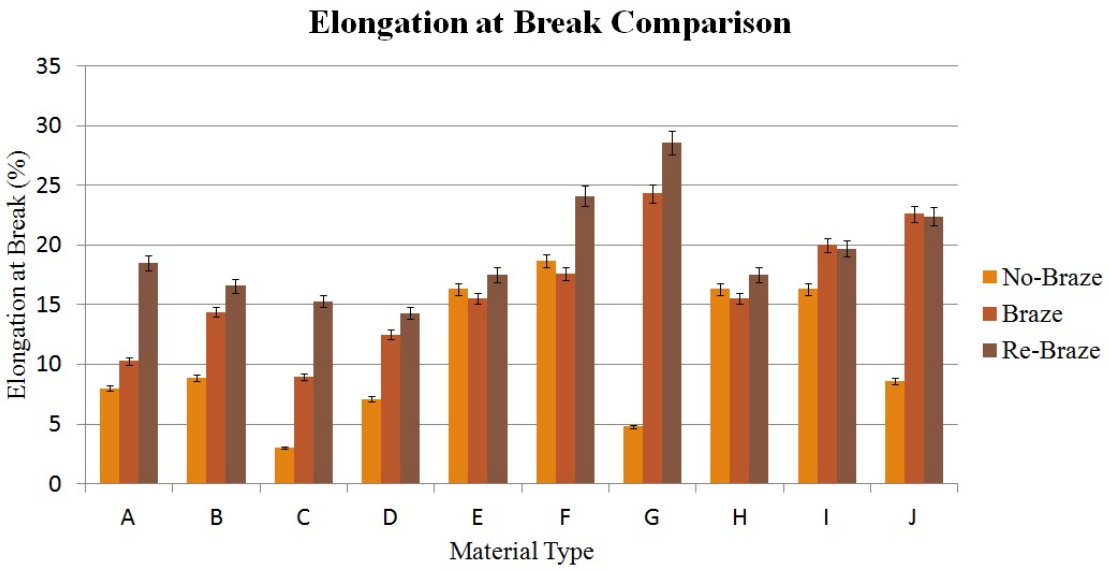

Fig. 4.6. Graphical representation of Elongation at Break comparison between the test materials.

That is why there could be see a significant drop in the properties from before brazing to after brazing. It could be assumed based on results obtained for the after re-braze case that the insignificant change in the ultimate tensile strength and yield strength on compared with after braze case could be because of grain size still being around the same size of the after braze material. But without microscopic images it is not possible to have a strong evidence on this claim. The standard deviation bars in the Fig. 4.4, Fig. 4.5 and Fig. 4.6 appear to be similar to the respective cases. It is because the deviation is not very high and the scale of the graph limits in identifying the difference between them visually.

In a tensile test, the grains orient themselves according to their preferred directions of deformation. When grain has a lot of neighbors, this rotation is difficult which increases the strength of the material. On the other hand, if relatively lesser grains are present, this rotation is facilitated and a decrease in mechanical properties is observed. When the grain size is of the same order of magnitude as the thickness of the sample, its mechanical properties are increasingly dependent on the morphology

and orientation of the grains. The reduction in the number of grains in the thickness leads to a sharp decrease in the number and thus a decrease in elongation at break [96]. According to Lorenzino et al. it is essential to take into account the ratio of the number of grains and the thickness t / D, (with t the thickness and D the grain size) and not just the thickness or the single grain size of a material. Indeed, it has been shown that when the ratio T / D decreases and becomes less than 1, the Hall-Petch rule is no longer valid [97].

Also by further reducing the thickness of the material the overall performance and strength properties decrease on comparing between the before braze and after braze of the material. For example, Dai et al. have carried out fatigue tests in strain imposed samples in pure copper with a constant grain size [98]. They studied the evolution of properties in fatigue by reducing the thickness of their samples without modifying the grain size. It was found that the reduction in thickness from 150 to 40 μm results in a decrease in the endurance limit to 106 cycles, thus confirming the trend observed by Lorenzino et al. on the AA1050 alloy. It is to be noted that the results of the literature in this field are very few.

As discussed above, commercial aluminum alloys of the 3XXX series contain dispersants of type Al_6 (Mn, Fe) and above all α-Al (Mn, Fe) Si [99]. These are generally considered inconsistent with the aluminum matrix. However, a crystallographic study has shown that type dispersoids A-Al (Mn, Fe) Si are partially coherent with the aluminum matrix [100]. We can be able to correlate the elasticity and fracture limits of aluminum samples of castings having undergone different heat treatments, difference of radius and fraction volume ratio of these dispersoids. The best properties in terms of elastic limit and limit at break are obtained after annealing at 375°C, which corresponds to the highest density of dispersoids. Thus, with a good combination of time and annealing temperature, the mechanical properties of the 3XXX series can be significantly increased with higher Manganese and Silicon concentration [101]. This effect, although significant, is limited by the relatively low volume fraction of the dispersoids at room temperature. The dispersoids have an effective means of in-

creasing the mechanical properties at high temperatures [102]. Indeed dispersoids are stable even at high temperatures (300°C), which gives good mechanical properties and resistance to creep compared to other structurally hardened aluminum alloys.

The addition of 0.7 to 1.2% of Mn makes it possible to increase significantly the elastic limit and to break without losing in ductility [103]. The Al_6Mn type dispersoids act as a barrier to the propagation of the dislocations and moreover lead to a change of sliding system towards a deflected slip system (uniform deformation). Thanks to the homogenization of the deformation, fatigue crack initiation will be delayed and results in improved fatigue life of alloys containing these dispersoids.

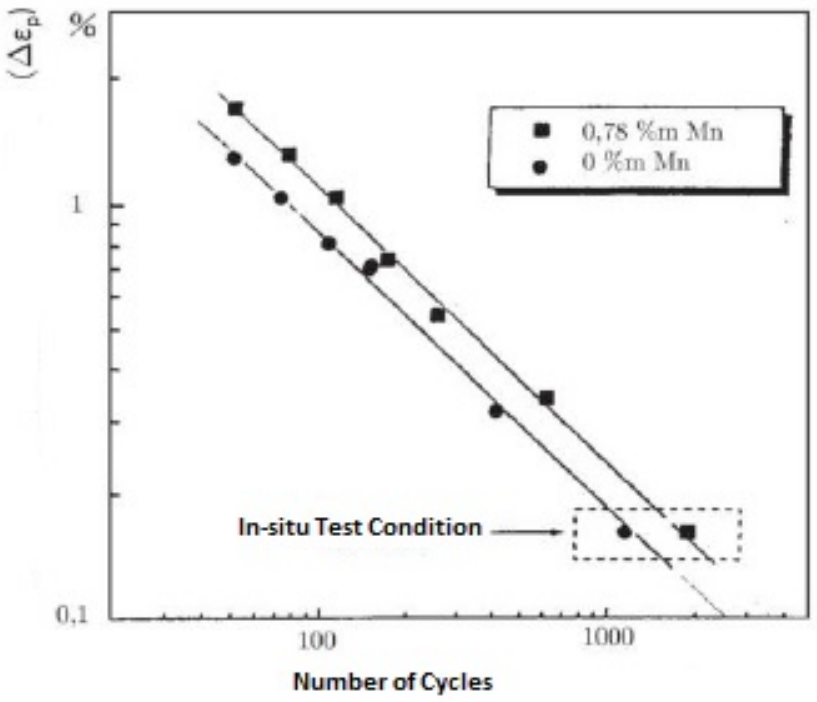

Fig. 4.7. Effect of manganese on the fatigue strength of a 7XXX alloy [104]

5. CONCLUSION AND FUTURE RECOMMENDATIONS

This study was carried out in the simple case of amplitude uniaxial loading of imposed constraint. The results show that the plastic deformation starts to occur after brazing at much lower stress levels than when before brazing. With the yield strength similar or no significant variation in the re-brazed materials while compared with the brazed materials, it is evident that there is not much impact on the plasticity and elasticity of the materials. Irrespective of the varying composition of the materials and the thickness of the test materials being different in all the cases, the trend in the properties studied do not have any significant effect. Also the Young's Modulus of the material sample shown in Fig. 4.1, Fig. 4.2 and Fig. 4.3 shows that the Young's Modulus drop as we continue braze and re-braze. In order to be more representative of the stresses on the tubes of radiator in operation, in particular during thermal shocks, it would be desirable to set up the tests in the deformation imposed. Attempts have already been made in this direction with the uniaxial loading. The specification of car manufacturers is becoming more and more stringent relates to the mechanical properties of the brazed heat exchangers. They are now to undergo ever greater temperature variations from -30°C to 120°C, corresponding to increasingly applied constraints. In order to ensure their perfect operation and avoid any cracking of tubes, several actions or studies can be considered.

Moreover this work was carried out at room temperature. Having revealed that, it would be ideal to have the tests performed in the temperature range between -30°C and 120°C to get close to realistic testing as similar to the actual thermal shocks the radiators are expected to go through. Nevertheless, as explained in previous chapters a similar tests were carried out by other researchers in understanding the mechanisms of damage between -30°C and 120°C and have proven the damage mechanisms do not change significantly as compared to the tests carried out essentially at ambient

temperature. The initial results obtained on comparison with the braze and re-braze data, it is promising and gives confidence on further developing a in depth understanding of microstructural level of re-braze material to see the feasibility of having re-brazing as a process without compromising mechanical properties.

From a material point of view it is the plating at 4045 which, when penetrating into the core during brazing weakens the material and reduces its strength properties of resistance. If the mechanisms could be observed and confirmed imposing deformation, two ways could be explored.

The first concerns will be the brazing conditions. It is this condition which will determine the surface state and the final microstructure of the material. In order to optimize them and to limit the penetration of the residual plating into the core, a detailed study of the microstructures obtained as a function of the temperature rise and cooling rates during brazing could be carried out (formation of intermetallic compounds in the grain boundaries).

The second is to try to minimize as much as possible the amount of clad on the tubes. It is not a matter of completely removing the 4045 but to find an optimum in order to guarantee a good brazability of the components while reducing the quantity of clad not used in the formation of joints. A strategy could be developed to reduce the quantity of filler metal supplied by the tubes and to increase the quantity of plating provided by the interlayers and the fins.

A study could be carried out to optimize the life of the exchangers as a goal in modifying the fragilizing microstructure after brazing at the surface of the tubes at the level of the 4045 clad alloy. The presence of fragile grain boundaries or core residual plating, brazed products of 4045 clad alloy with prime locations of failures could probably be minimized with a modification of the composition of the plating. The addition of alloying elements such as Strontium is known to produce Si needles with more rounded shapes [105]. The obtaining of globular and non-needle Si particles could make it possible to minimize their sensitivity to the stresses induced at the surface during a mechanical stress. In addition to the addition of Sr, the Fe, Mn values

of the 4045 plating could be the two other levers that could be used to modify the geometry of the intermetallics present at these same grain boundaries [106]. Finally, a study in crystalline plasticity could also be carried out in order to understanding of the mechanism of crack opening and their deviation by the second layer of grains.

Laboratory laminography is also a viable technique for monitoring cracking of macroscopic samples. This technique, which is complementary to the optics, makes it possible in particular to avoid the polishing of the specimens and to detect by volume damage.

REFERENCES

REFERENCES

[1] E. Schubert, M. Klassen, I. Zerner, C. Walz, and G. Sepold, "Light-weight structures produced by laser beam joining for future applications in automobile and aerospace industry," *Journal of Materials Processing Technology*, vol. 115, no. 1, pp. 2–8, 2001.

[2] G. Cole and A. Sherman, "Light weight materials for automotive applications," *Materials characterization*, vol. 35, no. 1, pp. 3–9, 1995.

[3] Y. Hisatomi, "Recent advance of brazing sheet and flux for aluminium brazing," *Welding International*, vol. 22, no. 7, pp. 421–426, 2008.

[4] S. Kahl, H.-E. Ekström, and J. Mendoza, "Tensile, fatigue, and creep properties of aluminum heat exchanger tube alloys for temperatures from 293 k to 573 k (20 c to 300 c)," *Metallurgical and Materials Transactions A*, vol. 45, no. 2, pp. 663–681, 2014.

[5] S. Tierce, "Etude de la corrosion des alliages d'aluminium brasés constituant les échangeurs thermiques utilisés dans les véhicules automobiles," Ph.D. dissertation, INPT, 2006.

[6] R. Benedictus, C. Keidel, G. Weber, and A. Haszler, "Method of producing a high strength balanced al-mg-si alloy and a weldable product of that alloy," Feb. 7 2006, "U.S. Patent 6,994,760".

[7] R. Kilmer, "Ultra-longlife, high formability brazing sheet," Aug. 14 2007, "U.S. Patent 7,255,932".

[8] R. K. Shah, "Advances in automotive heat exchanger technology," SAE Technical Paper, Tech. Rep., 2003.

[9] W. Miller, L. Zhuang, J. Bottema, A. Wittebrood, P. De Smet, A. Haszler, and A. Vieregge, "Recent development in aluminium alloys for the automotive industry," *Materials Science and Engineering: A*, vol. 280, no. 1, pp. 37–49, 2000.

[10] J. Paturaud, D. Fabrègue, J.-Y. Buffière, A.-G. Villemiane, and M. Perrier, "Résistance en fatigue en fonction de la température de feuilles d'aluminium brasées de fines épaisseur utilisées pour les échangeurs thermiques automobiles," *S21 Endommagement et rupture*, 2015.

[11] R. DEVELAY, "Propriétés de laluminium et de ses alliages," *Techniques de lingénieur COR*, vol. 325, pp. p1–21, 1992.

[12] D. Sichen, I. Arvanitidis, and S. Seetharaman, "Flux reactions in aluminum brazing with fluoride fluxes," *T*, vol. 96, p. 1042, 1996.

[13] C. Miller, "Fluxless aluminum brazing furnace," Aug. 12 1969, "U.S. Patent 3,460,816".

[14] W. Winterbottom and G. Gilmour, "Vacuum brazing of aluminum: Auger studies of wetting and flow characteristics," *Journal of vacuum Science and Technology*, vol. 13, no. 2, pp. 634–643, 1976.

[15] W. Cooke, T. Wright, and J. Hirschfield, "Furnace brazing of aluminum with a non-corrosive flux," SAE Technical Paper, Tech. Rep., 1978.

[16] W. Miller, L. Zhuang, J. Bottema, A. Wittebrood, P. De Smet, A. Haszler, and A. Vieregge, "Recent development in aluminium alloys for the automotive industry," *Materials Science and Engineering: A*, vol. 280, no. 1, pp. 37–49, 2000.

[17] P. Fortin, W. Kellermann, F. Smith, C. Rogers, and M. Wheeler, "Aluminum materials and processes for automotive heat exchanger applications," SAE Technical Paper, Tech. Rep., 1985.

[18] J. Liu, "Nocolok flux and aluminum brazing," SAE Technical Paper, Tech. Rep., 1996.

[19] M. Yamaguchi, H. Kawase, and H. Koyama, "Brazeability of al-mg alloys in non-corrosive flux brazing," *Furukawa review*, vol. 12, pp. 139–139, 1993.

[20] B. Wallis and U. Bentrup, "Zur thermischen entwässerung von k2alf5· h2o," *Zeitschrift für anorganische und allgemeine Chemie*, vol. 589, no. 1, pp. 221–227, 1990.

[21] D. Lauzon and H. Swidersky, "Myth about aluminium brazing with non-corrosive fluxes," 2002.

[22] J. E. Macintyre, *Dictionary of Inorganic Compounds, Supplement 4*. CRC Press, 1996, vol. 9.

[23] O. V. Kostrubsky, S. Mehta, and J. Noveskey, "Investigation of self-corrosion and galvanic compatibility of various components used in automotive condensers," in *Meeting Abstracts*, no. 14. The Electrochemical Society, 2006, pp. 768–768.

[24] C. Jeffcoate, M. Ranger, J. Grajzl, B. Yang, P. Woyciesjes, and A. Gershun, "Investigation of interaction between coolant formulations and flux loading/compositions in controlled atmosphere brazed (cab) aluminum surfaces in heat exchanger applications," *Journal of ASTM International*, vol. 4, no. 1, pp. 1–8, 2007.

[25] B. Yang, A. V. Gershun, F. J. Marinho, and P. M. Woyciesjes, "Effect of fluoride on corrosion of cooling system metals in ethylene glycol-based antifreeze/coolants," *Journal of ASTM International*, vol. 3, no. 10, pp. 1–10, 2006.

[26] J. Takigawa and T. Okamoto, "Materials and process factors in non-corrosive flux brazing for aluminum automobile heat exchangers." *KOBELCO TECHNOL REV.*, no. 16, pp. 34–38, 1993.

[27] R. Bolingbroke, A. Gray, and D. Lauzon, "Optimisation of nocolok (tm) brazing conditions for higher strength brazing sheet," SAE Technical Paper, Tech. Rep., 1997.

[28] M. Yamaguchi, H. Kawase, and H. Koyama, "Brazeability of al-mg alloys in non-corrosive flux brazing," *Furukawa review*, vol. 12, pp. 139–139, 1993.

[29] D. Lauzon and H. Swidersky, "Methods for minimizing or eliminating wastewater from flux slurries in non-corrosive flux brazing," SAE Technical Paper, Tech. Rep., 2001.

[30] J. Garcia, C. Massoulier, and P. Faille, "Brazeability of aluminum alloys containing magnesium by cab process using cesium flux," SAE Technical Paper, Tech. Rep., 2001.

[31] R. Kilmer, "Multi-layer, heat treatable brazing sheet with aluminum interlayer," Apr. 29 2003, "U.S. Patent 6,555,251".

[32] R. Benedictus, C. Keidel, G. Weber, and A. Haszler, "Method of producing a high strength balanced al-mg-si alloy and a weldable product of that alloy," Feb. 7 2006, "U.S. Patent 6,994,760".

[33] M. Pourbaix, "Atlas of electrochemical equilibria in aqueous solutions pergamon press ltd," *London, England*, 1966.

[34] M. Reboul, T. Warner, H. Mayet, and B. Baroux, "A ten-step mechanism for the pitting corrosion of aluminium," in *Materials Science Forum*, vol. 217. Trans Tech Publ, 1996, pp. 1553–1558.

[35] Z. Szklarska-Smialowska, "Pitting corrosion of aluminum," *Corrosion science*, vol. 41, no. 9, pp. 1743–1767, 1999.

[36] B. Baroux and D. Gorse, "Physique des films passifs," *CORROSION LOCALISEE, Les Editions de Physique*, pp. 91–147, 1994.

[37] F. Liang, R. Shi, E. Lazo, and M. Kozdras, "Electrochemical and corrosion performance of zinc-containing tri-layer aluminum brazing sheet aa7072/3003/4343 in oy synthetic water," SAE Technical Paper, Tech. Rep., 2005.

[38] D. Berges and F. Meslin, "The effect of nocolok potassiumfluoridezincate flux on evaporator corrosion resistance," SAE Technical Paper, Tech. Rep., 2005.

[39] A. G85-11, "Standard practice for modified salt spray (fog) testing," 2011.

[40] C. Vargel, "Corrosion de laluminium, paris: Dunod, 1999, 501 p," ISBN 2-100-04191-6, Tech. Rep.

[41] A. Kłyszewski, J. Żelechowski, A. Frontczak, P. Rutecki, W. Szymanski, Z. Zamkotowicz, and M. Nowak, "New rolled aluminium alloy products for the automotive industry," *Archives of Metallurgy and Materials*, vol. 59, no. 1, pp. 393–396, 2014.

[42] J. Garcia and D. Christian, "Correlations between charge air cooler (cac) distortion bench tests and flexion fatigue on test specimens," SAE Technical Paper, Tech. Rep., 2005.

[43] J. Yoon, S. Lee, and M. Kim, "Fabrication and brazeability of a three-layer 4343/3003/4343 aluminum clad sheet by rolling," *Journal of Materials Processing Technology*, vol. 111, no. 1, pp. 85–89, 2001.

[44] H. Philipps and P. Varley, "Equilibrium phase diagrams of aluminium alloy systems," *The aluminium Development Association*, 1961.

[45] A. Buteri, "Etude de l'endommagement en fatigue d'alliages d'aluminium brasés pour échangeurs thermiques automobiles," Ph.D. dissertation, INSA de Lyon, 2012.

[46] A. H. Properties, "Selection: Nonferrous alloys and special-purpose materials, vol. 2," *ASM International, Materials, Park, OH*, 1990.

[47] J. E. Hatch, A. Association *et al.*, *Aluminum: properties and physical metallurgy*. ASM International, 1984.

[48] Y. Li and L. Arnberg, "Evolution of eutectic intermetallic particles in dc-cast aa3003 alloy during heating and homogenization," *Materials Science and Engineering: A*, vol. 347, no. 1, pp. 130–135, 2003.

[49] D. Alexander and A. Greer, "Solid-state intermetallic phase tranformations in 3xxx aluminium alloys," *Acta Materialia*, vol. 50, no. 10, pp. 2571–2583, 2002.

[50] G. Marshall, A. Flemming, A. Gray, and R. Llewellyn, "Development of a long life aluminium brazing sheet alloy with enhanced mechanical performance," SAE Technical Paper, Tech. Rep., 1994.

[51] G. Marshall, R. Bolingbroke, and A. Gray, "Microstructural control in an aluminum core alloy for brazing sheet applications," *Metallurgical Transactions A*, vol. 24, no. 9, pp. 1935–1942, 1993.

[52] D. Alexander and A. Greer, "Nucleation of the al6 (fe, mn)-to-α-al–(fe, mn)–si transformation in 3xxx aluminium alloys. ii. transformation in cast aluminium alloys," *Philosophical Magazine*, vol. 84, no. 28, pp. 3071–3083, 2004.

[53] S. Tierce, N. Pébère, C. Blanc, G. Mankowski, H. Robidou, D. Vaumousse, and J. Lacaze, "Solidification and phase transformations in brazed aluminium alloys used in automotive heat exchangers," *International Journal of Cast Metals Research*, vol. 18, no. 6, pp. 370–376, 2005.

[54] J. Lacaze, S. Tierce, M.-C. Lafont, Y. Thebault, N. Pébère, G. Mankowski, C. Blanc, H. Robidou, D. Vaumousse, and D. Daloz, "Study of the microstructure resulting from brazed aluminium materials used in heat exchangers," *Materials Science and Engineering: A*, vol. 413, pp. 317–321, 2005.

[55] P. Fortin, P. Marois, and D. Evans, "Process for improving the corrosion resistance of brazing sheet," Aug. 20 1991, "U.S. Patent 5,041,343".

[56] R. Benedictus, S. Meijers, A. Wittebrood, and J. De Wit, "Influence of alloying additions on corrosion behavior of aluminum brazing sheet," in *Proc. 6th Int. Conf. on Aluminum Alloys (Tokyo, Japan: The Japan Institute of Light Metals, 1998)*, 1998.

[57] C. Sigli, L. Maenner, C. Sztur, and R. Shahani, "Phase diagram, solidification and heat treatment of aluminum alloys," in *ICAA-6: 6 th International Conference on Aluminium Alloys, Toyohashi, Japan, 5-10 Japan 1998*, 1998, pp. 87–98.

[58] S. Tierce, N. Pébère, C. Blanc, C. Casenave, G. Mankowski, and H. Robidou, "Corrosion behaviour of brazed multilayer material aa4343/aa3003/aa4343: Influence of coolant parameters," *Corrosion Science*, vol. 49, no. 12, pp. 4581–4593, 2007.

[59] D. Alexander, R. Hamerton, H. Cama, and A. Greer, "Investigating the alpha transformationa solid-state phase change of dispersed intermetallic particles from an al6 (fe, mn) phase to an α-al-(fe, mn)-si phase," in *Essential Readings in Light Metals*. Springer, 2016, pp. 1015–1020.

[60] M. Warmuzek, G. Mrówka, and J. Sieniawski, "Influence of the heat treatment on the precipitation of the intermetallic phases in commercial almn1fesi alloy," *Journal of Materials Processing Technology*, vol. 157, pp. 624–632, 2004.

[61] S. Tierce, "Etude de la corrosion des alliages d'aluminium brasés constituant les échangeurs thermiques utilisés dans les véhicules automobiles," Ph.D. dissertation, INPT, 2006.

[62] D. P. Sekulic, B. P. Zellmer, and N. Nigro, "Influence of joint topology on the formation of brazed joints," *Modelling and Simulation in Materials Science and Engineering*, vol. 9, no. 5, p. 357, 2001.

[63] D. Sekulic, P. Galenko, M. Krivilyov, L. Walker, and F. Gao, "Dendritic growth in al–si alloys during brazing. part 1: Experimental evidence and kinetics," *International journal of heat and mass transfer*, vol. 48, no. 12, pp. 2372–2384, 2005.

[64] D. Sekulic, P. Galenko, M. Krivlyov, L. Walker, and F. Gao, "Dendritic growth in al–si alloys during brazing. part 2: Computational modeling," *International journal of heat and mass transfer*, vol. 48, no. 12, pp. 2385–2396, 2005.

[65] M. Dehmas, P. Weisbecker, G. Geandier, P. Archambault, and E. Aeby-Gautier, "Experimental study of phase transformations in 3003 aluminium alloys during heating by in situ high energy x-ray synchrotron radiation," *Journal of alloys and compounds*, vol. 400, no. 1, pp. 116–124, 2005.

[66] B. P. Zellmer, N. Nigro, and D. P. Sekulic, "Numerical modelling and experimental verification of the formation of 2d and 3d brazed joints," *Modelling and Simulation in Materials Science and Engineering*, vol. 9, no. 5, p. 339, 2001.

[67] F. Gao, D. P. Sekulic, Y. Qian, and X. Ma, "Residual clad formation and aluminum brazed joint topology prediction," *Materials Letters*, vol. 57, no. 29, pp. 4592–4596, 2003.

[68] M. Kral, "A crystallographic identification of intermetallic phases in al–si alloys," *Materials Letters*, vol. 59, no. 18, pp. 2271–2276, 2005.

[69] M. Dehmas, R. Valdés, M.-C. Lafont, J. Lacaze, and B. Viguier, "Identification of intermetallic precipitates formed during re-solidification of brazed aluminium alloys," *Scripta materialia*, vol. 55, no. 2, pp. 191–194, 2006.

[70] M. Nylén, U. Gustavsson, W. B. Hutchinson, and A. Örtnäs, "Mechanistic studies of brazing in clad aluminium alloys," in *Materials Science Forum*, vol. 217. Trans Tech Publ, 1996, pp. 1703–1708.

[71] D. Schmatz, "Grain boundary penetration during brazing of aluminum," *Welding Journal*, vol. 62, no. 10, pp. 267–271, 1983.

[72] S.-H. Kim, J.-H. Kang, K. Euh, and H.-W. Kim, "Grain-structure evolution of brazing-treated a4343/a3003/a4343 aluminum brazing sheets rolled with different reductions," *Metals and Materials International*, vol. 21, no. 2, p. 276, 2015.

[73] H. Nayeb-Hashemi and M. Lockwood, "The effect of processing variables on the microstructures and properties of aluminum brazed joints," *Journal of materials science*, vol. 37, no. 17, pp. 3705–3713, 2002.

[74] A. J. Wittebrood, "Microstructural changes in brazing sheet due to solid-liquid interaction," Ph.D. dissertation, TU Delft, Delft University of Technology, 2009.

[75] R. A. Woods, "Liquid film migration during aluminum brazing," SAE Technical Paper, Tech. Rep., 1997.

[76] H. H. S. Yang and R. A. Woods, "Mechanisms of liquid film migration (lfm) in aluminum brazing sheet," SAE Technical Paper, Tech. Rep., 1997.

[77] M. Nylen, U. Gustavsson, W. B. Hutchinson, and Å. Karlsson, "The mechanism of braze metal penetration by migration of liquid films in aluminium," in *Materials science forum*, vol. 331. Trans Tech Publ, 2000, pp. 1737–1742.

[78] M. Kuo and R. Fournelle, "Diffusion induced grain boundary migration (digm) and liquid film migration (lfm) in an al-2.07 wt% cu alloy," *Acta metallurgica et materialia*, vol. 39, no. 11, pp. 2835–2845, 1991.

[79] K.-R. Lee, Y.-J. Baik, and D. N. Yoon, "A critical test for the coherency strain energy as the driving force for the discontinuous precipitation in mo-ni alloy," *Acta Metallurgica*, vol. 35, no. 8, pp. 2145–2150, 1987.

[80] D. Yoon, "Theories and observations of chemically induced interface migration," *International materials reviews*, vol. 40, no. 4, pp. 149–179, 1995.

[81] S. Suresh, *Fatigue of materials*. Cambridge university press, 1998.

[82] J. Chaboche, C. Bathias, and J. Baïlon, "La fatigue des matériaux et des structures," *Hermès*, pp. 617–644, 1997.

[83] W. Yu, Z. Xingguo, M. Linggang, Z. He, Z. Min, and J. Nan, "The microstructure and properties evolution of al–si/al–mn clad sheet during plastic deformation," *Journal of Materials Research*, vol. 28, no. 12, pp. 1601–1608, 2013.

[84] Q. Zhao and B. Holmedal, "The effect of silicon on the strengthening and work hardening of aluminum at room temperature," *Materials Science and Engineering: A*, vol. 563, pp. 147–151, 2013.

[85] N. Liu, J. Jie, Y. Lu, L. Wu, Y. Fu, and T. Li, "Characteristics of clad aluminum hollow billet prepared by horizontal continuous casting," *Journal of Materials Processing Technology*, vol. 214, no. 1, pp. 60–66, 2014.

[86] P. B. Roy, F. M. OConnell, T. H. Callahan, E. J. Armellino, and W. L. Elban, "Vickers microindentation hardness testing of brazed joints in aluminum," 2013.

[87] M. Edo, M. Enomoto, and Y. Takayama, "Fatigue and creep properties of al–si brazing filler metals," in *ICAA13: 13th International Conference on Aluminum Alloys*. John Wiley & Sons, Inc., 2012, pp. 737–742.

[88] T. Fujii, H. Shintate, H. Yaguchi, H. Mitani, A. Inada, K. Shinkai, S. Kumai, and M. Kato, "Microstructural development during fatigue of a polycrystalline 3003 aluminum alloy," *ISIJ international*, vol. 37, no. 12, pp. 1230–1236, 1997.

[89] T. Fujii, C. Watanabe, Y. Nomura, N. Tanaka, and M. Kato, "Microstructural evolution during low cycle fatigue of a 3003 aluminum alloy," *Materials Science and Engineering: A*, vol. 319, pp. 592–596, 2001.

[90] H. Yaguchi, H. Mitani, K. Nagano, T. Fujii, and M. Kato, "Fatigue-damage evaluation in aluminum heat-transfer tubes by measuring dislocation cell-wall thickness," *Materials Science and Engineering: A*, vol. 315, no. 1, pp. 189–194, 2001.

[91] H. E. Boyer *et al.*, *Atlas of fatigue curves*. Asm International, 1985.

[92] H.-H. Kim and S.-B. Lee, "Effect of a brazing process on mechanical and fatigue behavior of alclad aluminum 3005," *Journal of mechanical science and technology*, vol. 26, no. 7, pp. 2111–2115, 2012.

[93] X. Yao, R. Sandström, and T. Stenqvist, "Strain-controlled fatigue of a braze clad al–mn–mg alloy at room temperature and at 75 and 180 c," *Materials Science and Engineering: A*, vol. 267, no. 1, pp. 1–6, 1999.

[94] Y. Bergström, "A dislocation model for the stress-strain behaviour of polycrystalline α-fe with special emphasis on the variation of the densities of mobile and immobile dislocations," *Materials Science and Engineering*, vol. 5, no. 4, pp. 193–200, 1970.

[95] A. Standard, "E8," standard test methods for tension testing of metallic materials," *Annual book of ASTM standards*, vol. 3, pp. 57–72, 2004.

[96] M. Klein, A. Hadrboletz, B. Weiss, and G. Khatibi, "The size effecton the stress–strain, fatigue and fracture properties of thin metallic foils," *Materials Science and Engineering: A*, vol. 319, pp. 924–928, 2001.

[97] M. Lederer, V. Gröger, G. Khatibi, and B. Weiss, "Size dependency of mechanical properties of high purity aluminium foils," *Materials Science and Engineering: A*, vol. 527, no. 3, pp. 590–599, 2010.

[98] C. Dai, B. Zhang, J. Xu, and G. Zhang, "On size effects on fatigue properties of metal foils at micrometer scales," *Materials Science and Engineering: A*, vol. 575, pp. 217–222, 2013.

[99] A. M. F. Muggerud, "Transmission electron microscopy studies of dispersoids and constituent phases in al-mn-fe-si alloys," Ph.D. dissertation, Skipnes Kommunikasjon as, 2014.

[100] Y. Li, A. Muggerud, A. Olsen, and T. Furu, "Precipitation of partially coherent α-al (mn, fe) si dispersoids and their strengthening effect in aa 3003 alloy," *Acta Materialia*, vol. 60, no. 3, pp. 1004–1014, 2012.

[101] A. M. F. Muggerud, E. A. Mørtsell, Y. Li, and R. Holmestad, "Dispersoid strengthening in aa3xxx alloys with varying mn and si content during annealing at low temperatures," *Materials Science and Engineering: A*, vol. 567, pp. 21–28, 2013.

[102] K. Liu and X.-G. Chen, "Development of al–mn–mg 3004 alloy for applications at elevated temperature via dispersoid strengthening," *Materials & Design*, vol. 84, pp. 340–350, 2015.

[103] S. W. Nam and D. H. Lee, "The effect of mn on the mechanical behavior of al alloys," *Metals and Materials International*, vol. 6, no. 1, pp. 13–16, 2000.

[104] K. Kim and S. Nam, "Effects of mn-dispersoids on the fatigue mechanism in an al–zn–mg alloy," *Materials Science and Engineering: A*, vol. 244, no. 2, pp. 257–262, 1998.

[105] M. Haque and A. F. Ismail, "Effect of superheating temperatures on microstructure and properties of strontium modified aluminium–silicon eutectic alloy," *Journal of materials processing technology*, vol. 162, pp. 312–316, 2005.

[106] A. Samuel and F. Samuel, "Modification of iron intermetallics by magnesium and strontium in al-si alloys," *International Journal of Cast Metals Research*, vol. 10, no. 3, pp. 147–157, 1997.